Final Technical Report

Federal Agency & Organization: Department of Energy

Award Number: DOE DE-FE0023031

Project Title: Distributed fiber sensing systems for 3D combustion temperature field monitoring in coal-fired boilers using optically generated acoustic waves

Program Managers: Barbara Carney and Jessica Mullen

PIs: Xingwei Wang[1], Professor, Xingwei_Wang@uml.edu, 978-934-1981
Chengyu Cao[2], Associate Professor, ccao@engr.uconn.edu, 860-486-3487
Xinsheng Lou[3], Technology Leader, xinsheng.lou@ge.com

Postdoc Researchers: Nan Wu[1] and Poorna Marthi[1]

Ph.D. Students: Jingcheng Zhou[1], Xu Guo[1], Cong Du[1], Tong Ma[2] and Yuqian Liu[2]

Master Students: Siwen Bi[1] and Rachana Guruprasad Kashyap[1]

DUNS Number: 956072490

Recipient Organization: [1]University of Massachusetts Lowell, [2]University of Connecticut, [3]GE Power

Project Location: [1]University of Massachusetts Lowell, Ball Hall 403, One University Ave, Lowell, MA 01854

[2]University of Connecticut, 191 Auditorium Road, E2 104 Storrs, CT 06269

[3]GE Power, 175 Addison Rd, Windsor, CT 06095

Reporting Period: September 1, 2014 to December 31, 2018

Signature: Susan C. Puryear Digitally signed by Susan C. Puryear DN: cn=Susan C. Puryear, o=University of Massachusetts Lowell, ou=Executive Director, Office of Research Administration, email=susan_puryear@uml.edu, c=US Date: 2019.04.11 15:38:24 -04'00'

Susan C, Puryear
Executive Director, Office of Research Administration

IMPORTANT NOTE: If any part of your final report contains proprietary/confidential information, or details that should not be released to the general public, the specific sections of the report should be marked as such, by clearly marking the beginning and end of the confidential information. The marked sections will not be released to the general public or any unauthorized parties.

Table of Contents

1 Executive Summary

In this project, we have developed and tested three kinds of fiber optic sensing systems for real time monitoring of temperature variations within an industrial scale boiler furnace. The fiber optic sensing systems target spatial and temporal distributions of high temperature profiles in a boiler furnace in fossil power plants. The reconstructed temperature profile will provide critical input for the control mechanisms to optimize the combustion process. This temperature profile will address the essential problem for fossil power plants in achieving higher efficiency and fewer pollutant emissions.

Acoustic pyrometer systems have been used to reconstruct temperature field of power plant boilers based on measuring TOF (times-of-flight) of sound waves along some straight paths in a 2D cross-section of the boiler. In this project, optically generated acoustic signals from a fiber optic sensing system have replaced the acoustic signals generated from an electrical transducer. A 3D reconstruction algorithm replaced the previous 2D model.

In this project, three kinds of fiber optic sensing systems have been developed and tested. They are fiber optic sensing system I, fiber optic sensing system II (Distributed Sensing System I) and fiber optic sensing system III (Distributed Sensing System II).

For fiber optic sensing system I, the fiber optic ultrasound generator acts as a signal generator. A microphone, hydrophone or other electronic devices serve as a signal receiver. In this system, there are one generator and one receiver. Distance test, water temperature test, air temperature test, air temperature reconstruction, and GE ISBF pilot test were performed by Fiber optic sensing system I. The fiber optic sensing system I successfully detected temperature in all these tests. We got 2D temperature reconstruction results by using the fiber optic sensing system I and it matched the reference data. The fiber optic sensing system I successfully survived in GE ISBF boiler environment (480 °F).

For fiber optic sensing system II (Distributed Sensing System I), it is an all optical ultrasound system. The fiber optic ultrasound generator acts as a signal generator. Fiber Bragg Grating (FBG) and Fabry-Perot (FP) sensor act as a signal receiver. In this system, there is one generator and one receiver. Aluminum plate temperature test, furnace high temperature test, and GE ISBF pilot test were performed by the fiber optic sensing system II. Fiber optic sensing system II successfully detected the temperature in all these tests. The fiber optic sensing system II successfully survived at up to 700 °C furnace environment and 320 °C GE ISBF boiler environment.

For fiber optic sensing system III (Distributed Sensing System II), it is also an all optical ultrasound system. The fiber optic ultrasound generator acts as a signal generator. Multiple FP fiber sensors act as signal receivers. In this system, there is one generator and three receivers. Three GE ISBF pilot tests were performed by fiber optic sensing system III. The fiber optic sensing system III survived in the cold flow tests in GE's ISBF pilot test facility. However, we didn't get high temperature data by using this system since the nanosecond laser issues.

During the period of the project, test trials, data simulation and algorithm optimization was performed successfully. For real time temperature field construction, the sampling rate must be fast enough to capture the field variations. The technology of Code-division multiple access (CDMA) is well studied which could allow parallel multiplexing, even if signals overlap in time or frequencies. Moreover, it has been known that extending the length of signal significantly improves SNR. For acoustic signals, these multiplexing techniques have also been widely used, mainly for sonar and acoustic communications. The CDMA modulation technique has been proposed and studied to guarantee high network throughput, low channel access delay and low energy consumption.

We have studied the temperature field reconstruction using Gaussian Radial Basis Functions (GRBF)-based approximation approach. Reconstruction of 3D temperature field using Neural Networks with measured TOF and known propagation paths is feasible. 2D and 3D temperature field reconstruction simulation results are achieved.

The milestone status is shown in Table 1. We finished milestone 1-8 and milestone 10. For milestone 9, we did three pilot tests by using the fiber optic sensing system III (Distributed Sensing System II) at GE Power. However, due to the failure of the ns laser, we did not get the temperature results. We conducted some additional tasks that were not originally proposed: 1) We fabricated a fiber optic sensing system I and did a pilot test based on this system. 2) In the proposal, we proposed two pilot tests at GE Power. In reality, we finished at least seven pilot tests at GE Power. GE Power has made a lot of efforts for supporting the pilot tests. 3) We got a simulation results based on CDMA.

In summary, most of the tasks have been accomplished. The outcome of this project removed a few barriers that hinder the achievement of the final product of the distributed sensing systems. With the successful accomplishment of this project, a prototype of the fiber optic sensing system can be fabricated to attract more interests from companies and other funding agencies.

Table 1. Milestone Status Report

Milestone Title/ Description	**Planned Completion Date**	**Actual Completion Date**	**Completion Percentage**	**Verification Method**	**Comments (Progress toward achieving milestone, explanation of deviation from plan, etc.)**
M1/Develop Project Management Plan	July, 2014	July, 2014	100%	Plan Submission to DOE	This task is completed.
M2/ Establish a Simulation Model for Furnace Temperature Profile	January, 2015	January, 2015	100%	Simulation Program Files	This task is completed.
M3/Clarify Requirements for Distributed Sensing System Design	April, 2015	April, 2015	100%	Requirements Report	This task is completed.
M4/Develop Active Sensing Element	April, 2016	April, 2016	100%	Working Prototype	This task is completed.
M5/Characterize Distributed Sensing System I	April, 2016	April, 2016	100%	Working Prototype	This task is completed.

M6/Develop Reconstruction Algorithm	April, 2016	April, 2016	100%	2D and 3D simulations using Matlab	This task is completed.
M7/Facility Test Distributed Sensing System I at GE Power	July, 2016	July, 2016	100%	Test Report	This task is completed.
M8/Develop Distributed Sensing System II	January, 2017	January, 2017	100%	Working Prototype	This task is completed.
M9/Facility Test Distributed Sensing System II at GE Power	May, 2018	February, 2019	100%	Test Report	We did three pilot tests by using the Fiber Optic Sensing System III (Distributed Sensing System II) at GE Power. We achieved 1) Cold flow test on GE's ISBF pilot test facility. 2) FP fiber sensor survived in hot flow test on GE's ISBF pilot test facility.
M10/Develop Final Report	June, 2018	March, 2019	100%	Deliver Final Report to DOE	This task is completed.

2 Significance

Fiber optic sensing systems are novel distributed optical fiber sensing systems for real-time monitoring and optimization of spatial and temporal distributions of high temperature profiles, such as in boiler furnaces in fossil power plants. These are the first active, non-contact, all optical fiber distributed sensing systems to use optically generated acoustic signals to operate in the harsh environments of coal-fired power generation systems. The reconstructed 3D temperature profiles can provide critical inputs for the control mechanisms to optimize the combustion processes. These systems can address the critical problem in fossil power plants in achieving higher efficiency and fewer pollutant emissions. Table 2 compares our Fiber optic sensing system characteristics with other types of temperature sensors.

The purpose of this project is to develop a novel low cost distributed optical fiber sensing system for real-time monitoring and optimization of spatial and temporal distributions of high temperature profiles in a boiler furnace in a fossil power plant as shown in Fig. 1 and Fig. 2. This project features by high novelty in the sensing and data processing methods. This is the first active non-contact all optical fiber distributed sensing system to use optically generated acoustic signals to operate in the super harsh environment of coal generation systems. The work has a great significance because of the ability of the distributed fiber sensors to survive high temperatures and the ability of the optically generated acoustic signals to measure even

higher temperature profiles where the fibers do not reach. The reconstructed 3D temperature profile will provide critical input for the control mechanisms to optimize the combustion process. This will address the critical problem in fossil energy power plants of achieving higher efficiency and fewer pollutant emissions. Since it is a non-contact measurement approach, extremely high temperatures (up to 2000 °C) could be remotely measured. The distributed fiber optic sensors themselves can operate in temperatures of up to 700 °C, and the temperature resolution can be smaller than 10 °C when using special fibers (such as Sapphire). This work is the first step in a continuum of research, and silica optical fibers will be used to develop this novel sensor system.

Table 2. Temperature sensor characteristics

	Fiber optic sensing system	**Thermo-couples (TCs)**	**Resistance Temperature Devices (RTDs)**	**Thermistors General Purpose**	**Infrared Pyrometer**	**Semiconductor Temperature Sensor**	**Distributed PZT sensing systems**
Sensor configuration	3D temperature distribution	Single point	Single point	Single point	Single point	Single point	3D temperature distribution
Temperature Range	Remotely measure up to 2000 ºC Survive in temperatures up to 700 ºC	Up to 2300 ºC	Up to 850 ºC	Up to 125 ºC	Up to 3300 ºC	Up to 125 ºC	Remotely measure up to 2000 ºC Survive in temperatures up to 100 ºC
Sensitivity	High	Medium	Low	High	High	High	High
Size packaging (General)	Small	Small to Large	Small to Medium	Small to Large	Medium	Small	Medium
Company name	UMass	Omega	Omega	Omega	Omega	Mouser Electronics	Enertechnix
Model number	UMass FOS	Super OMEGACLAD™ XL Thermoco-uple Probes	General Purpose RTD (PT100) PR-10	General Purpose Thermistor TH-10-44000	Dual Laser Infrared Thermometer OS768-LS	ON Semiconductor NCT375	PyroMetrix ™ Acoustic Pyrometer
Size /packaging (Specific)	One Generator or Receiver Dimensions: 20 mm × 20 mm × 20 mm [Estimate]	Probe Diameters: 1.5 ~ 9.5 mm Probe Length: 150 mm ~ 600 mm	Probe Diameters: 3 ~ 6 mm Probe Length: 150 mm ~ 600 mm	Probe Diameters: 4.5 ~ 6 mm Probe Length: 50 mm ~ 100 mm	Dimensions: 204 mm × 179 mm × 58 mm	Dimensions: 2.3 mm × 1.3 mm × 0.9 mm	One Generator or Receiver Dimensions: At least 200 mm × 200 mm × 200 mm [Estimate]

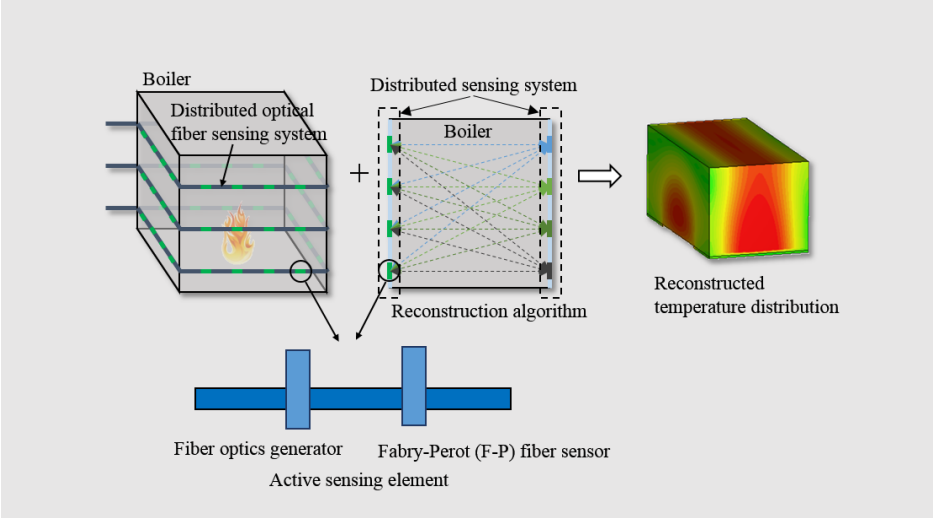

Fig. 1. The objective of the proposed project: Reconstruct the 3D high temperature distribution within a boiler via a novel fiber optic distributed temperature sensing system using optically generated acoustic waves.

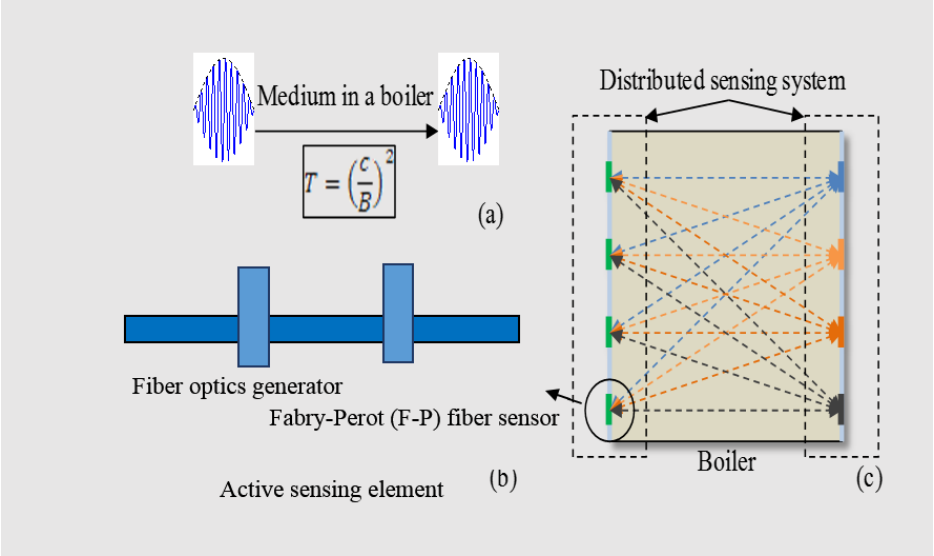

Fig. 2. The principle of the temperature measurement. (a) The temperature is determined by the speed of the sound. (b) The schematic diagram of one sensing element. (c) The schematic diagram of the temperature distribution reconstruction.

3 Project Results

3.1 Generators and receivers. (Milestone 3 and Milestone 4)

3.1.1 Tip generators and Sidewall generators

Fiber optic ultrasound generators are based on the photoacoustic principle, which uses optical signals to generate ultrasound waves. Fiber optic ultrasound generators are easy to fabricate. A fiber optic tip generator structure is illustrated in Fig. 3. Gold nanocomposite material coated at the fiber end is used as the photo-absorptive material. Fiber optic sidewall generators structure are illustrated in Fig. 4. Ultrasound signals generated by the fiber optic generators are shown in Fig. 5.

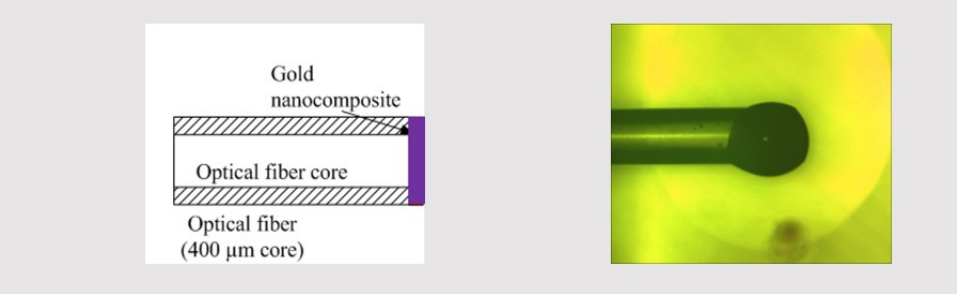

Fig. 3. Fiber optic tip generator structure

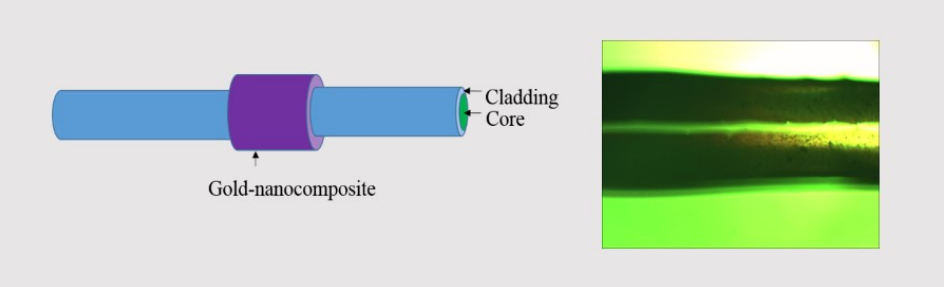

Fig. 4. Fiber optic sidewall generator structure

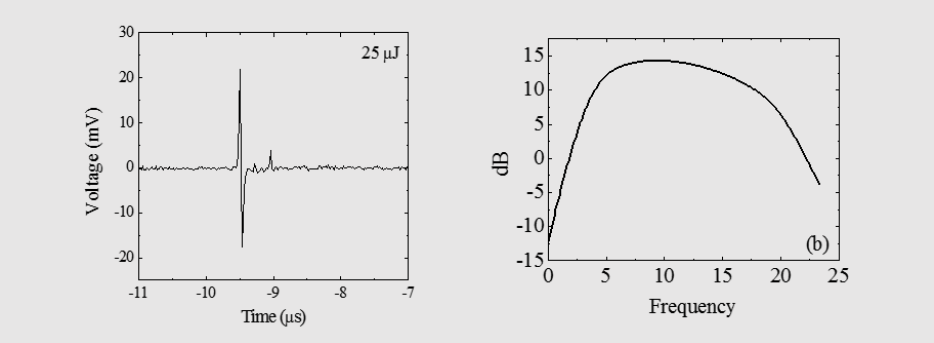

Fig. 5. Time and frequency domain of ultrasound signals

3.1.2 Fiber Bragg Grating (FBG) receiver and Fabry-Perot (FP) receiver.

1) Fiber Bragg Grating (FBG) receiver

FBG receivers were commercially obtained. The comparison of FBG receiver performance with hydrophone is shown in Fig. 6. The comparison test was performed under water. PZT was used as the signal generator. FBG receiver and hydrophone was used as the signal receiver. The FBG receiver and hydrophone were frequency matched. This indicates that FBG receivers can be used to detect the ultrasound signal in water.

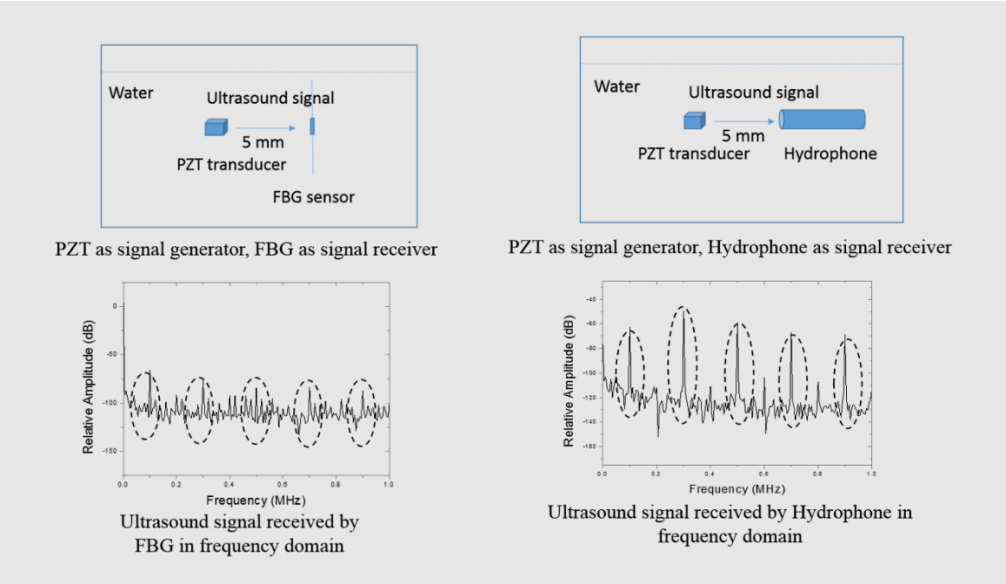

Fig. 6. FBG receiver performance comparison with hydrophone

2) Fabry-Perot (FP) receiver I

Fabry-Perot (FP) receiver I is based on Fabry-Perot principle. The FP receiver I is easy to fabricate. Structure and packaging of the FP receiver are shown in Fig. 7. FP receiver I performance comparison with microphone is shown in Fig. 8. In the comparison test, a fiber optic tip generator was used as the signal generator. The FP receiver I and a microphone were used as the signal receivers. The FP receiver I detected the same results as the microphone for different distances. It shows that the FP receiver I can be used to detect the ultrasound signal in air.

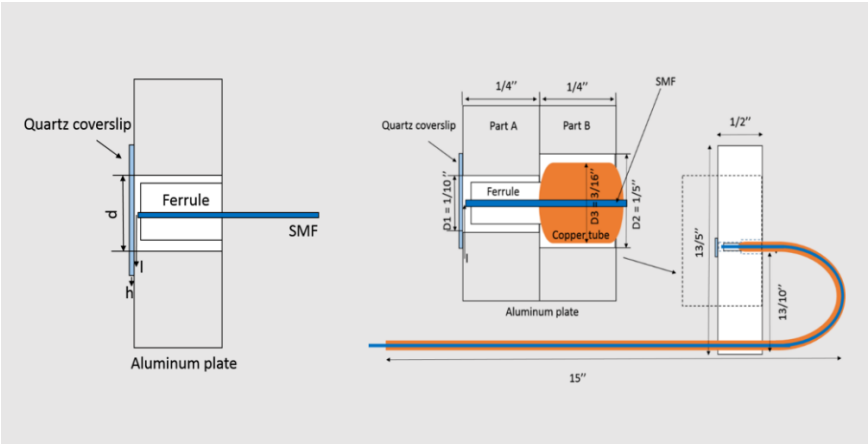

Fig. 7. Structure and packaging of FP receiver I.

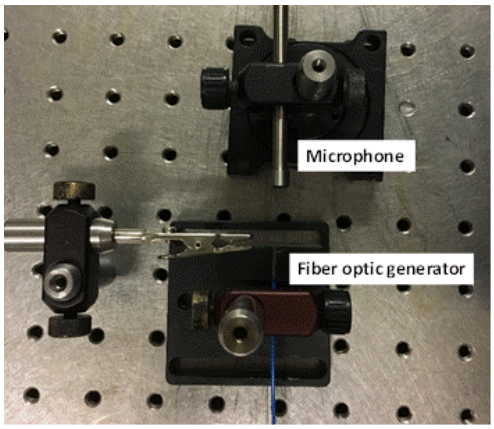

(a)

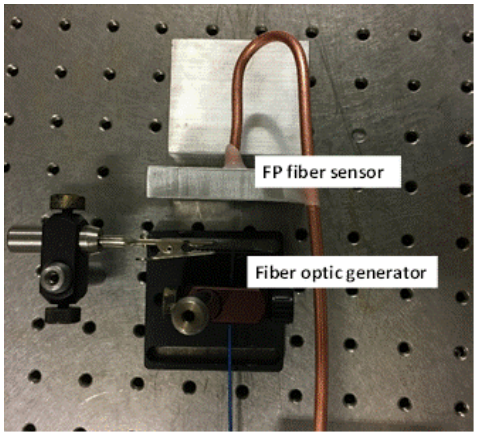

(b)

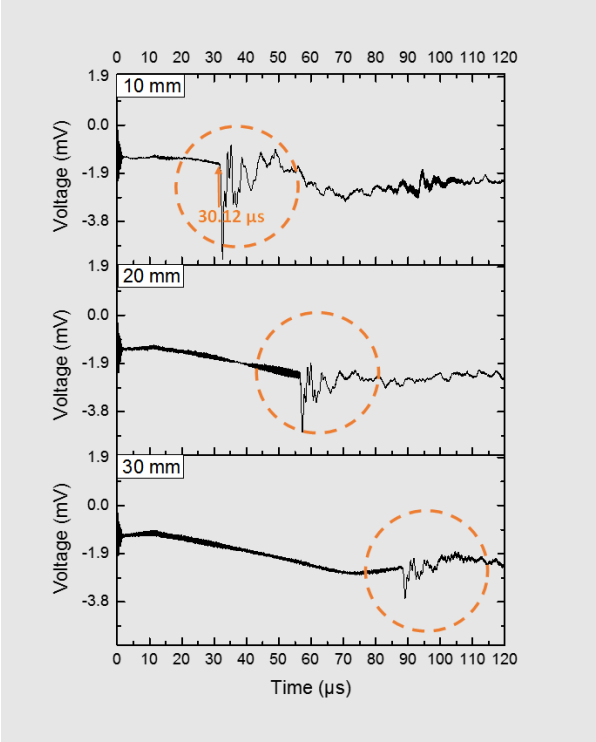

(c)

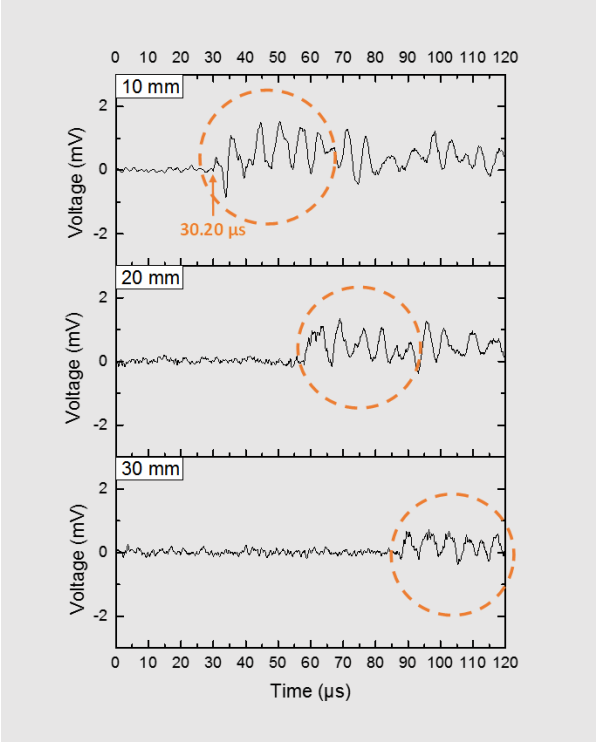

(d)

Fig. 8. FP receiver I performance comparison with microphone. (a) Experimental setup for the fiber optic generator and microphone system. (b) Experimental setup for the fiber optic generator and FP sensor system. (c) The ultrasonic signal detected by the microphone. (d) The ultrasonic signal detected by the FP fiber sensor.

3) Fabry-Perot (FP) receiver II

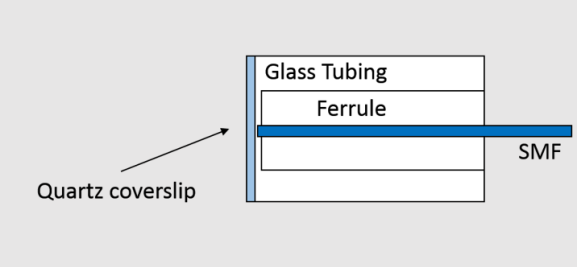

Fig. 9. Structure of FP receiver II.

The structure of FP receiver II is shown in Fig. 9. A 2.7 mm inner dimension glass tubing replaced the previous aluminum disc to increase the sensitivity and reduce the size of the receiver as shown in Fig. 9. Spectrums of the four FP receiver IIs are shown in Fig. 10.

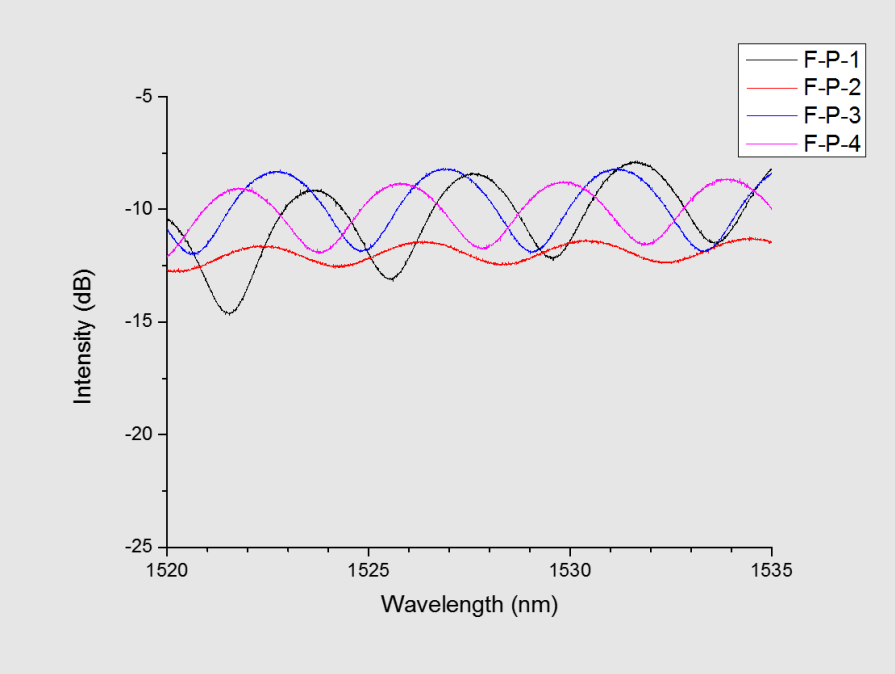

Fig. 10. Spectrums of four FP fiber receiver IIs.

An FP receiver II sensitivity test was performed as shown in Fig. 11. A black PDMS coated 1000/1035 μm fiber generator was used as a signal generator. An FP receiver II (FP-1) was used in this test. The wavelength of tunable laser was set at 1525 nm. The distance between the generator and the receiver was fixed at 5 mm.

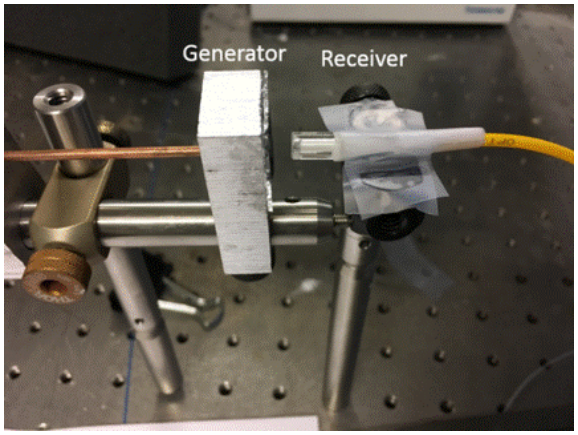

Fig. 11. FP fiber receiver II sensibility test.

The testing result is shown in Fig. 12. The ultrasound travel time is 14 μs; 14 μs × 340 m/s = 4.8 mm. The Vpp is around 7 mV, which is 1.4 times to the previous FP fiber sensor. Based on the sensitivity equation 1,

$$Y_c = \frac{3(1-\mu^2)(d/2)^4}{16Eh^3} \cdot 10^9 \quad (1)$$

E is the quartz's Young's modulus, μ is the quartz Poisson ratio, h is the thickness of the quartz coverslip, d is the inner dimension of the glass tubing. While the d increase from 2.54 to 2.7 mm, the sensitivity should increase to (2.7/2.54)×4 =1.3 which matched the test results.

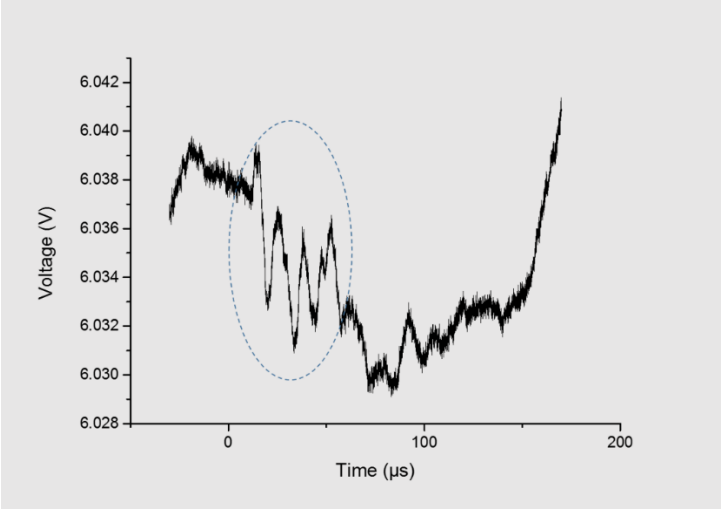

Fig. 12. FP receiver II test results.

3.2 Fiber optic sensing system I.

In fiber optic sensing system I, fiber optic ultrasound generator act as a signal generator and microphone, hydrophone or other electronic device act as a signal receiver. Many tests have been conducted by using fiber optic sensing system I.

3.2.1 Fiber optic sensing system I distance test.

This test was to measure the testing distance of fiber optic sensing system I in air condition. The experimental setup is shown in Fig. 13. The fiber optic ultrasound generator was used as the signal generator and a microphone (2670, Brüel & Kjær Sound &Vibration Measurement A/S) was used as a signal receiver. Ultrasound signals were generated by a photoacoustic material, which is the black PDMS in this case. An optical fiber with 600 µm as the core diameter was used to guide the laser to the glass slide. The distance between the generator and the receiver was set as 22 cm, 30 cm, 60 cm, 80 cm and 100 cm respectively. The test results are shown in Fig. 14. The fiber optic sensing system I can detect the ultrasound signal when the distance was set to 100 cm (1 meter).

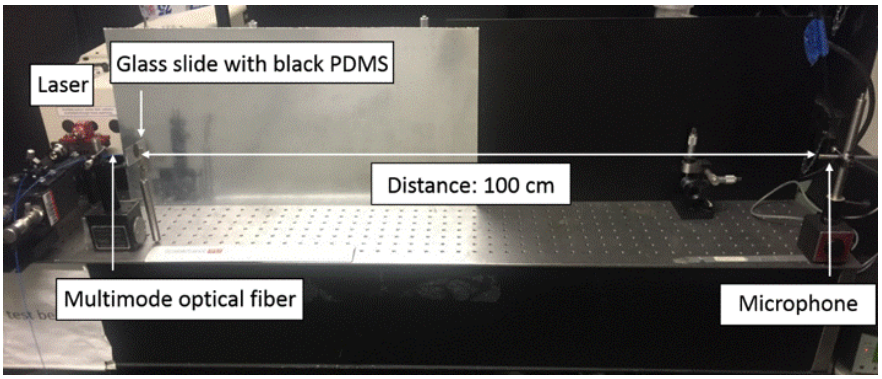

Fig. 13. Fiber optic sensing system I distance test.

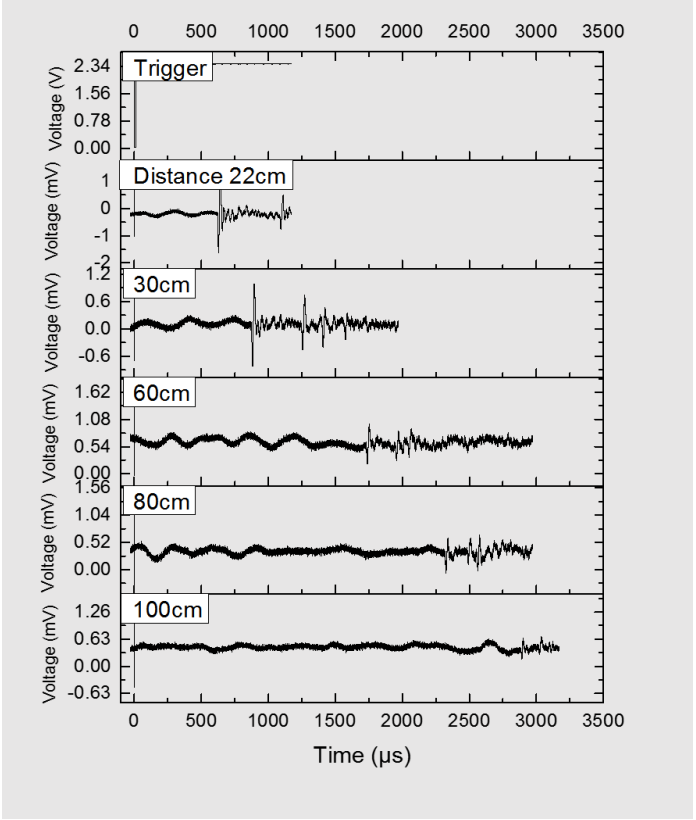

Fig. 14. Fiber optic sensing system I distance test results.

3.2.2 Fiber optic sensing system I water temperature test.

This test was to use the fiber optic sensing system I to measure the temperature of pure water environments. The experimental setup is shown in Fig. 15. The fiber optic ultrasound generator was used as the signal generator and a hydrophone was used as the signal receiver. The water temperature was changed from 13 °C to 45°C. The experimental results are compared with the simulation results as shown in Fig. 16. It demonstrates the temperature measurement capability of the Fiber optic sensing system I in water.

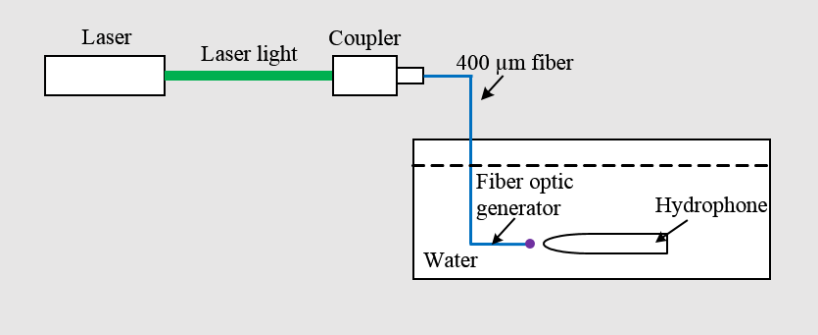

Fig. 15. Experimental setup for the water temperature measurement

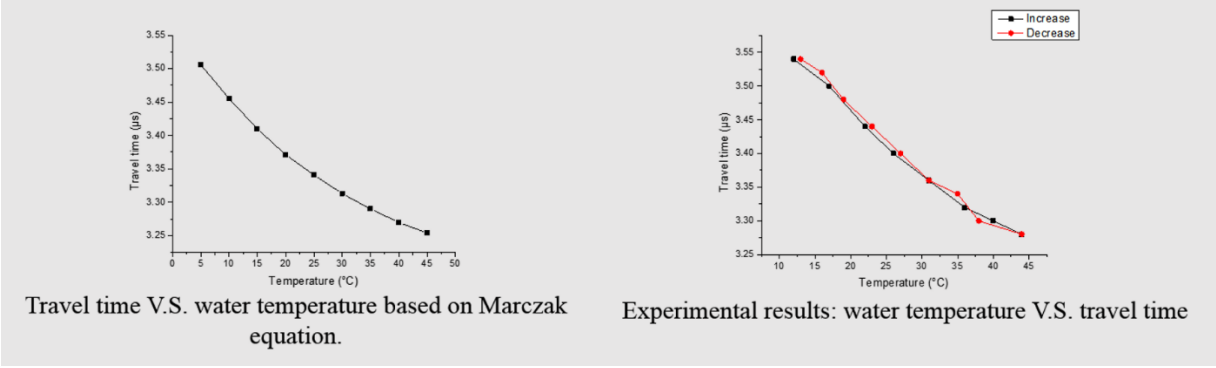

Travel time V.S. water temperature based on Marczak equation.

Experimental results: water temperature V.S. travel time

Fig. 16. Experimental results were compared with the simulation results

3.2.3 Fiber optic sensing system I air temperature test and reconstruction.

1) Air temperature test

This test was to use the fiber optic sensing system I to measure the temperature of air. The experimental setup is shown in Fig. 17. A fiber optic ultrasound generator was used as the signal generator and a microphone was used as the signal receiver. A candle with a flame was used as the measurement target which was set in the center of a 20 cm × 20 cm area. There were 12 positions along this chamber square area, where the signal generator and the receiver were placed. After acoustic signals propagated through multiple paths, the ultrasound signals were acquired. Ultrasound signal between positions 2 and 8 was shown in Fig. 18. There are two signals which are with flame and without flame. The travel time of the signal has big difference between flame and without flame, which demonstrated the temperature measurement capability of this fiber optic sensing system I in air.

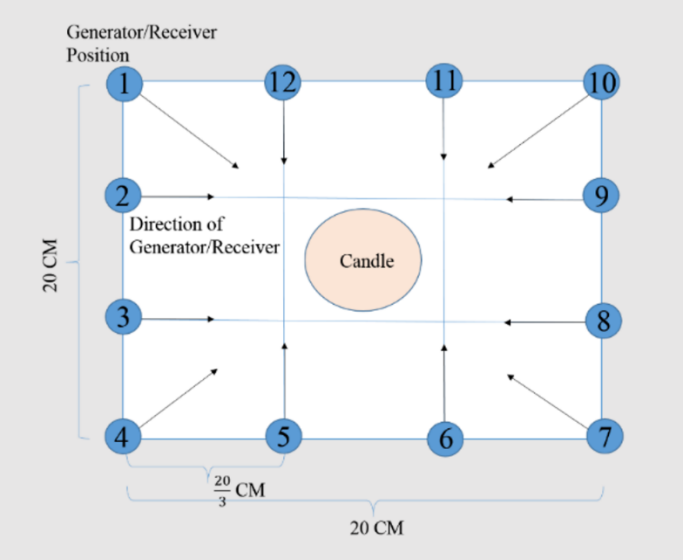

Fig. 17. Experimental setup for the air temperature measurement.

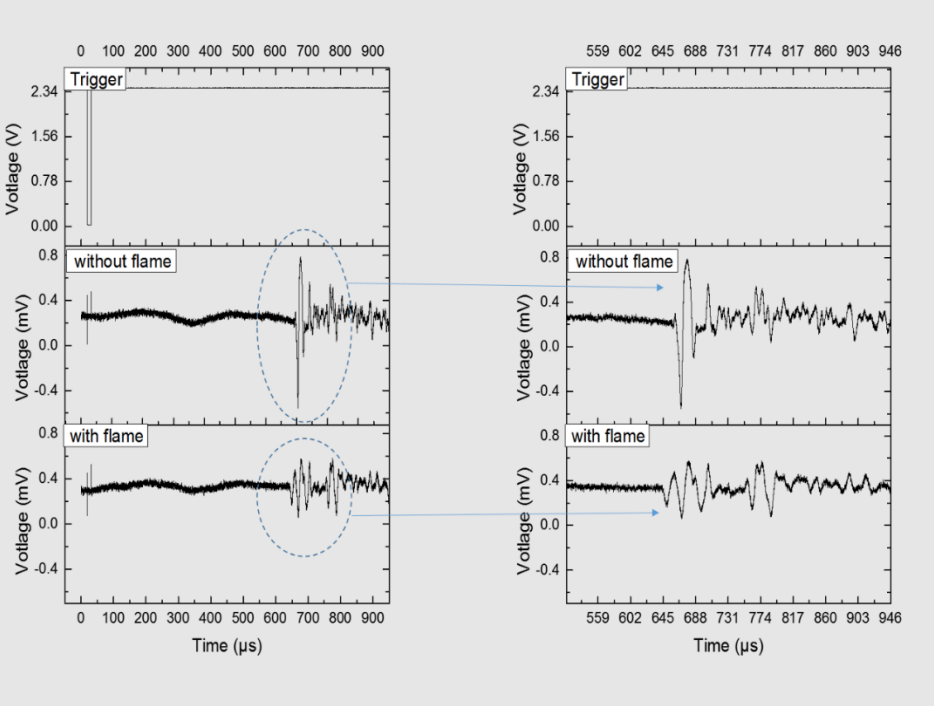

Fig. 18. Ultrasound signals between position 2 and position 8

2) Air temperature reconstruction

This test was to use the fiber optic sensing system I to measure the temperature in air and reconstructed the temperature distribution. The experimental setup is shown in Fig. 19. Ultrasound signals were generated by a photoacoustic material, which is the black PDMS in this case. An optical fiber with 1 mm as the core diameter was used to guide the laser to the glass slide. A microphone (PCB, 130C21) receiver was used as the signal receiver. The generator and receiver were fixed on the two moving stages. The height of generator

and receiver was also same. The test was performed outside of a lab furnace. The furnace temperature was set as 250 ºC.

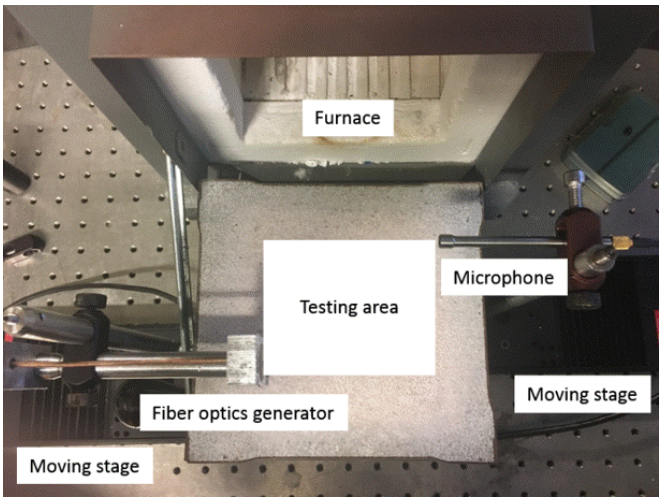

Fig. 19. Experimental setup.

The testing area is shown in the Fig. 20. It is a rectangle area (8cm × 6cm). The receiver (Microphone) was set on 5 different positions by using moving stage. The generator was set to 3 different positions. The blue points were the testing generator and receiver positions. 15 different paths were tested in the experiment as shown in Fig. 20. Data were collected at room temperature (26 ºC) and high temperature respectively. We set the generator position at 0, 0.5 and 1, the receiver position at 8, 7.5, 7, 6.5 and 6.

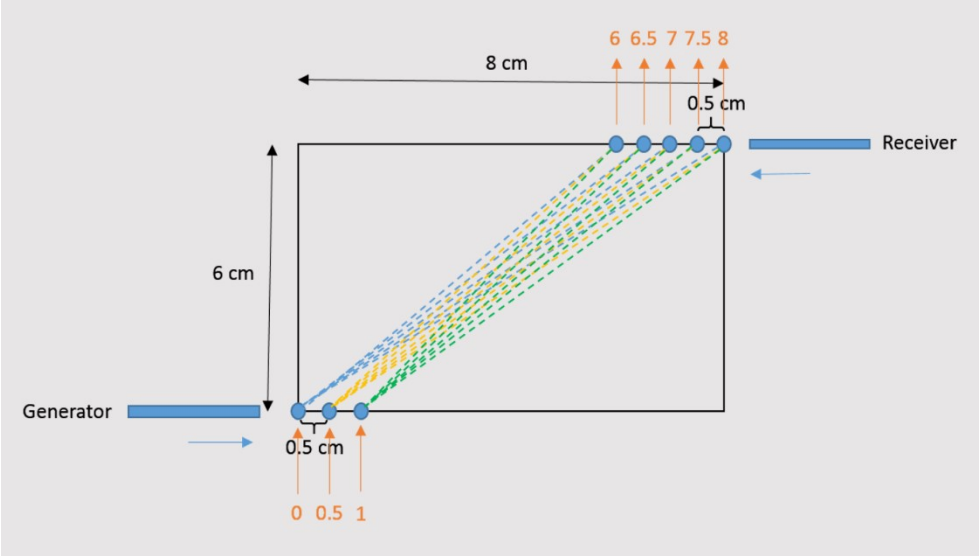

Fig. 20. Testing area.

As shown in Fig. 21, it was the position (0, 8) (generator at position 0 and receiver at position 8) data. The above one was ultrasound signal at room temperature (26 ºC). The below one was ultrasound signal at testing high temperature.

According the website (http://www.sengpielaudio.com/calculator-speedsound.htm) tool, we can calculate the sound speed was 346.71 m/s at 26 ºC. We can find the travel time was around 283 μs at room temperature. 346.71 m/s × 283 μs = 9.81 cm. We also can find the travel time was 276 μs at high temperature, so 9.81 cm/276 μs = 355.43 m/s. Based on the website tool, we can get the temperature is around 41.24 ºC. The average temperature for this path was around 42 ºC. 15 path temperatures were shown

in Table 3. The reference temperatures were shown in the Fig. 22. The reference temperature we measured by thermocouple were center temperatures of small cube area (2cm × 2cm). We used 15 path 1D temperature to reconstruct a 2D (yellow area shown in Fig. 23) temperature distribution. The reconstructed results are shown in Fig. 24 which matched the reference results.

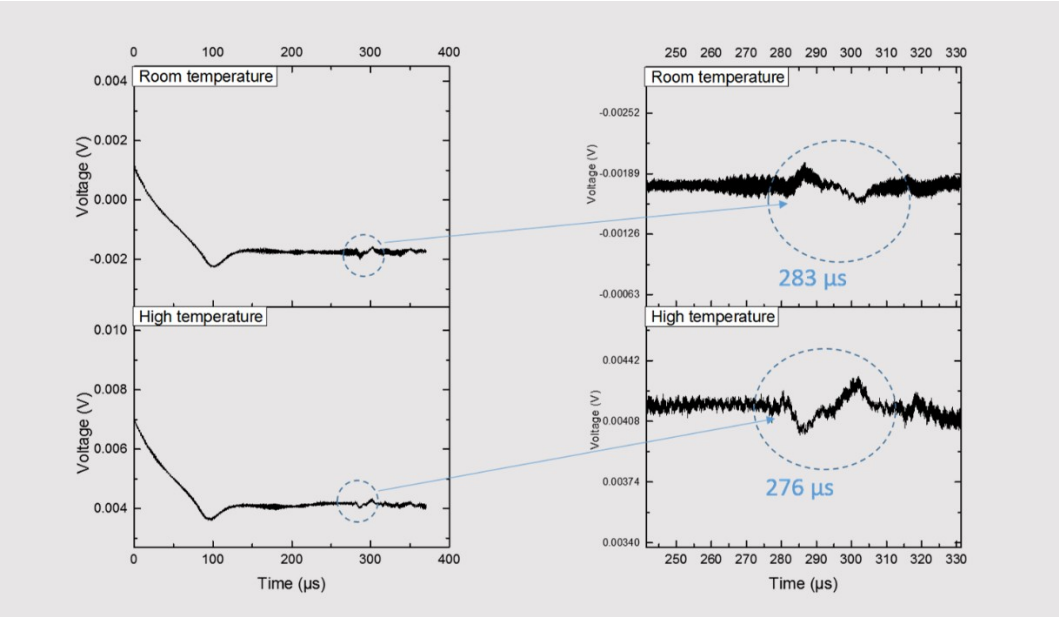

Fig. 21. Position (0, 8) ultrasound signal

Table 3. 15 paths temperature information

Position	Room Temperature Traveling Time (μs)	Testing Temperature Traveling Time (μs)	Average Temperature (°C)
(0, 8)	283	276	41.24
(0, 7.5)	271	267	35.02
(0, 7)	259	250	47.93
(0, 6.5)	247	244	33.40
(0, 6)	236	233	33.75
(0.5, 8)	270	264	39.75
(0.5, 7.5)	260	256	35.42
(0.5, 7)	248	242	41.02
(0.5, 6.5)	236	232	36.41
(0.5, 6)	224	219	39.82
(1, 8)	259	255	35.46
(1, 7.5)	248	244	35.89

(1, 7)	236	232	36.41
(1, 6.5)	225	221	36.93
(1,6)	215	211	37.45

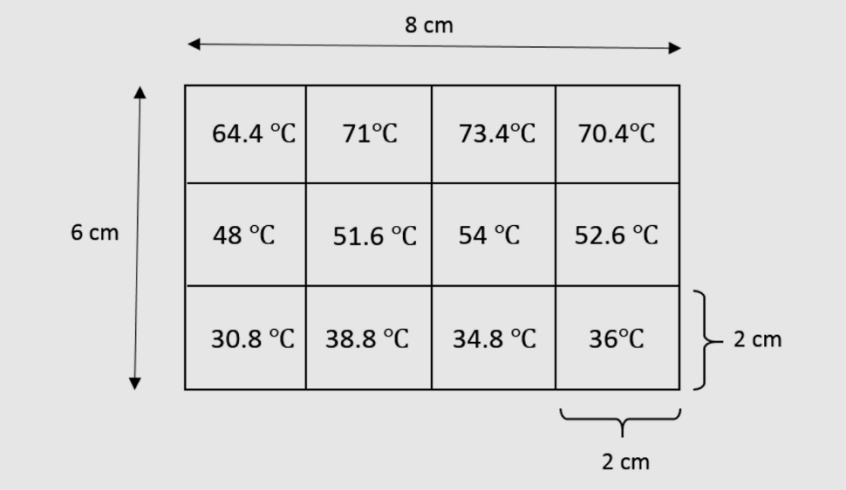

Fig. 22. Reference temperature.

We used 15 paths temperature data to reconstruct a 2D (yellow area shown in Fig. 23) temperature distribution. The reconstructed results are shown in Fig. 24 which matched the reference data.

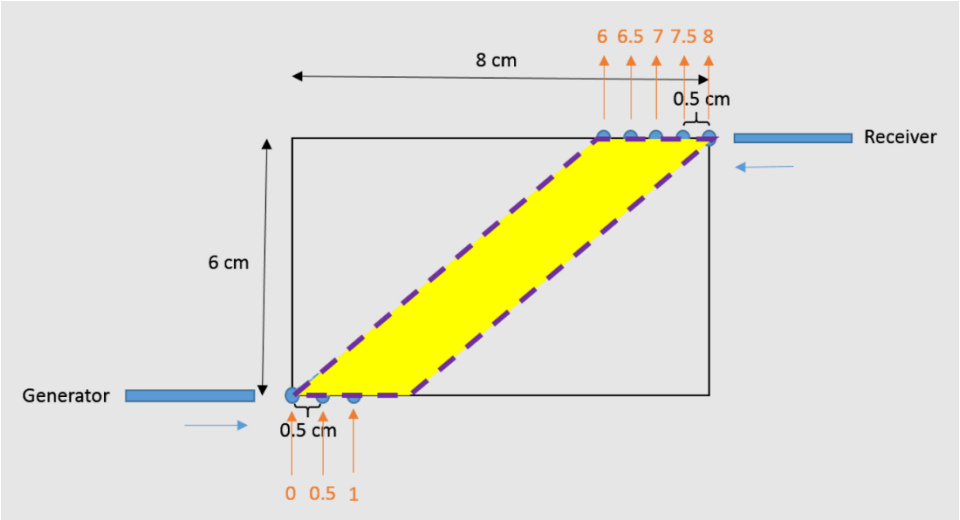

Fig. 23. Temperature reconstruction area.

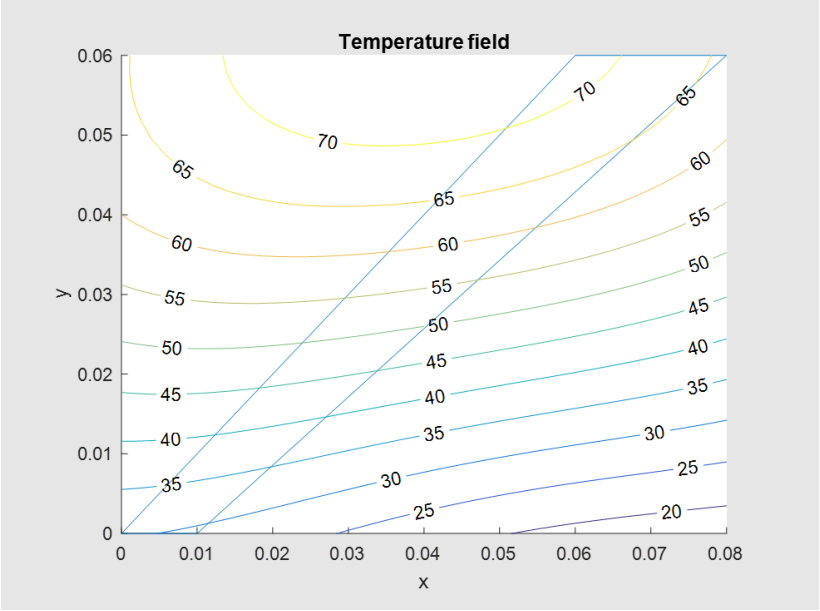

Fig. 24. Temperature field distribution in microphone.

3.3 Fiber optic sensing system II. (Milestone 5)

Fiber optic sensing system II is an all optical ultrasound system which the fiber optic ultrasound generator act as a signal generator and FBG or FP receiver act as a signal receiver. For the fiber optic sensing system II, one generator and one receiver was used in this system. Several tests had been done by using fiber optic sensing system II.

3.3.1 Fiber optic sensing system II aluminum plate temperature test.

This test was to use the Fiber optic sensing system II to measure the temperature on solid. The experimental setup is shown in Fig. 25. A fiber optic ultrasound generator was used as the signal generator, the FBG was used was the signal receiver. The ultrasound signal detected by the FBG in different temperature was shown in Fig. 26. It demonstrated the temperature measurement capability of the fiber optic ultrasound transducer system on solid.

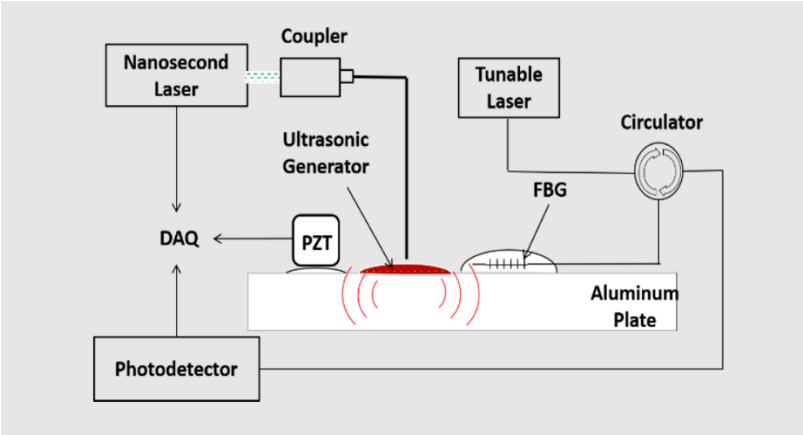

Fig. 25. Experimental setup for the aluminum plate temperature measurement

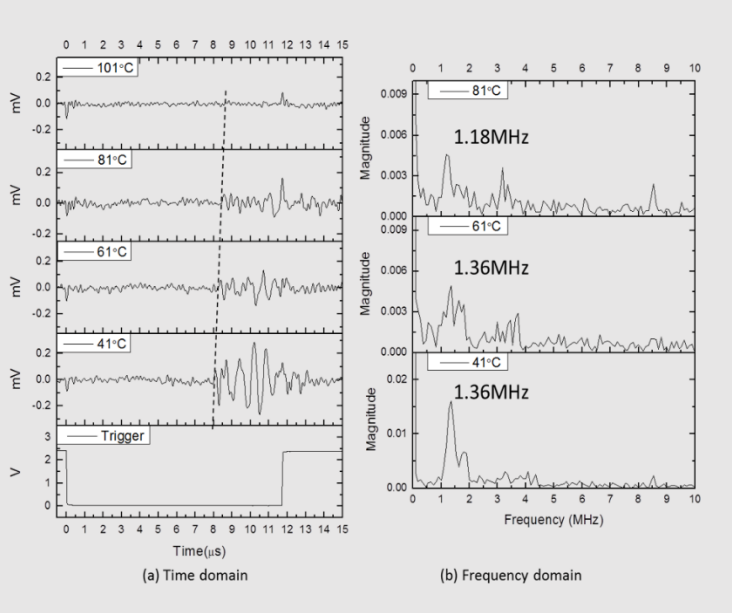

Fig. 26. Experimental results of aluminum plate temperature test in (a) time domain and (b) frequency domain by FBG

3.3.2 Fiber optic sensing system II furnace high temperature test.

This test was to test if the fiber optic ultrasound system II could be survived in very high temperature environment. The experimental setup is shown in Fig. 27 and Fig. 28. A fiber optic ultrasound generator was used as the signal generator, the FP receiver was used was the signal receiver. The furnace temperature was set at room temperature (24 ºC) to high temperature (700 ºC). The door of the furnace was covered by the aluminum foil. The water cooling system was used in this test. The Carbon Black slide was attached to the water block of the water cooling system. The FP receiver I (V20170321TEST1) was used as the signal receiver. The spectrum was shown in Fig. 29. The wavelength was set at 1565.7 nm. The distance between the generator and the receiver was fixed at 10 mm. Temperature between the generator and the receiver was recorded by a thermocouple (KHXL-116G-RSC-24, OMEGA).

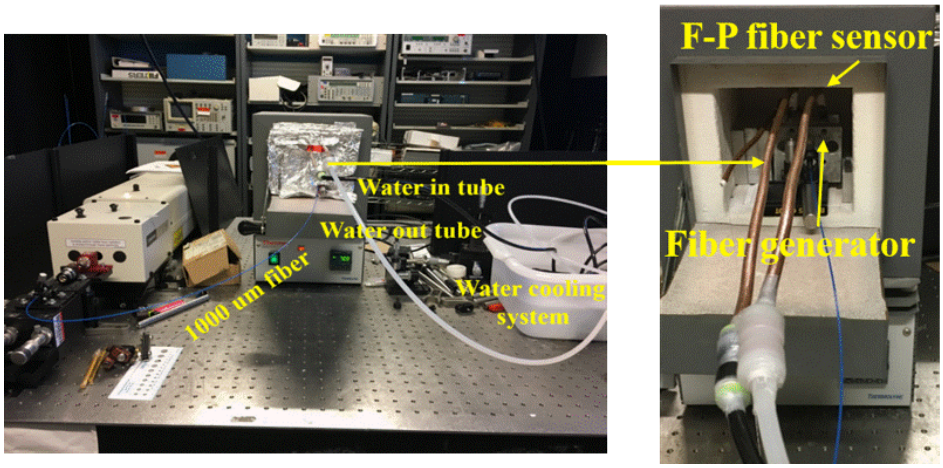

Fig. 27. Experimental setup for the furnace test.

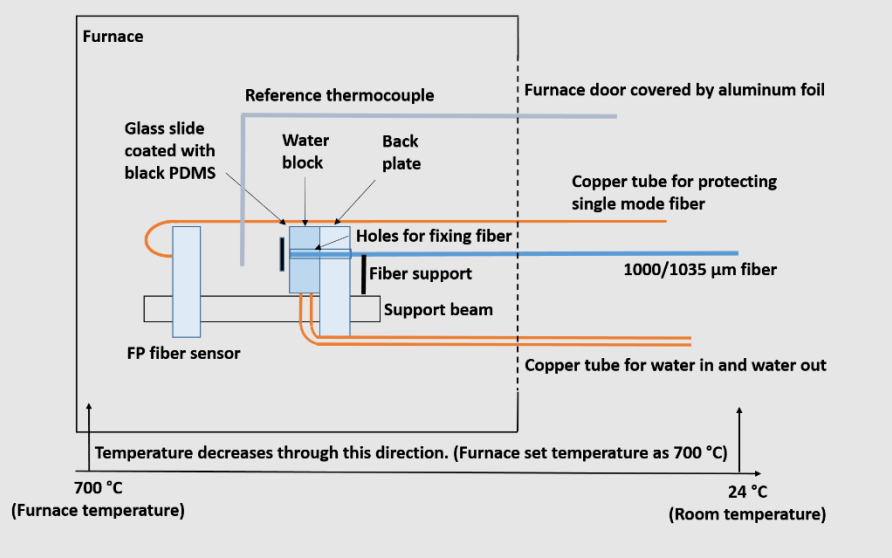

Fig. 28. Schematic of furnace test setup.

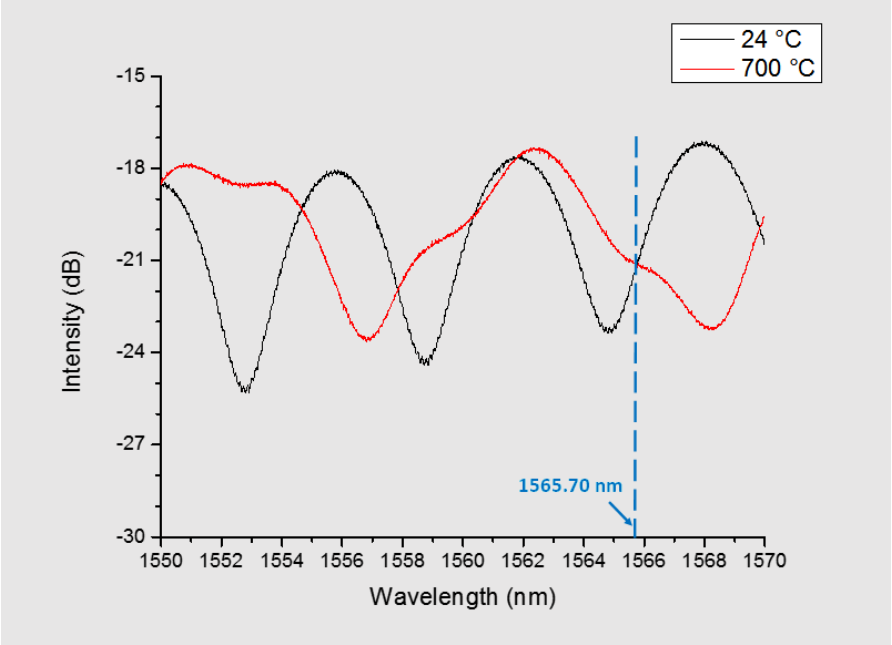

Fig. 29. Spectrum of the FP receiver I (V20170321TEST1) at a different temperature.

There was a clear ultrasound signal when the furnace setting temperature at 24 ºC (room temperature) and 700 ºC (high temperature). The FP fiber sensor spectrum became stable at 700 ºC after 20 minutes when the furnace reached its set temperature. It took 1 hour for the furnace to reach 700 ºC.

At 700 ºC, the spectrum of the FP fiber sensor had a big difference compared with that under room temperature. But the spectrum was stable. The ultrasound signal could be detected. The ultrasound signals are shown in Fig. 30 at 24 ºC (room temperature) and 700 ºC.

The travel time results and the furnace setting temperature, the thermocouple reference temperature, the cooling system water in and water out temperature information are listed in Table 4. Data were recorded for three times at 700 ºC test.

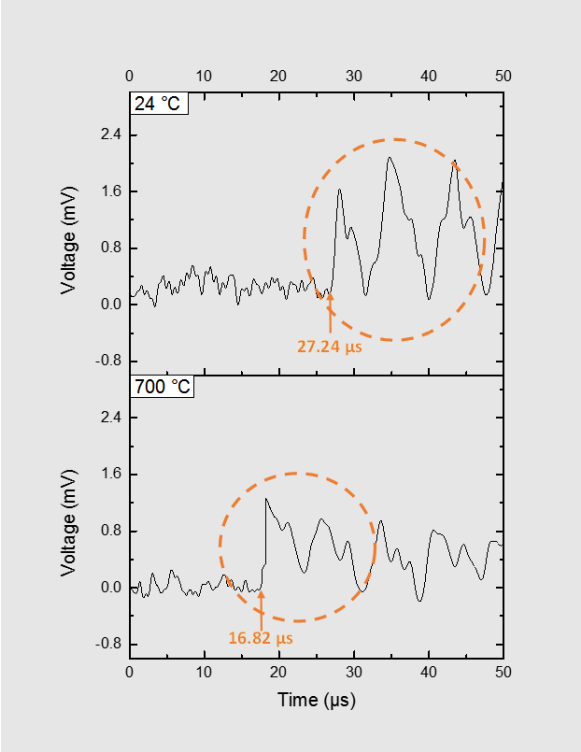

Fig. 30. Ultrasound signal when the furnace setting temperature at 24 ºC (room temperature) and 700 ºC, respectively.

Table 4. The relationship between different temperature results.

Furnace setting temperature (ºC)	Temperature reading between the generator and the receiver from a thermocouple (ºC)	Travel time from our optical system (μs)	Temperature calculated based on the travel time (ºC)	Water temperature at water tube in (ºC)	Water temperature at water tube out (ºC)
24	24	27.24	24	24	24
700	530	16.82	506.25	36.3	53.2
700	530	16.72	515.60	36.3	53.2
700	530	16.60	527.05	36.3	53.2

The temperature based on the optical system was calculated. One of the results were shown in Fig. 30. Since the distance between generator and receiver was not exactly 10 mm. The real distance could be calculated by multiply the sound speed and the travel time at room temperature. The sound speed was 345.549 m/s at 24 ºC (room temperature).

$$345.549\ \frac{m}{s} \times 27.24\ \mu s\ =\ 9.413\ \text{mm}$$

$\frac{9.413\ \text{mm}}{16.82\ \mu\text{s}} = 559.631\ \text{m/s}$, which was represented by 506.25 ºC according to the temperature and speed equation; (http://www.sengpielaudio.com/calculator-speedsound.htm)

The results at 700 ºC and other test results were shown in Fig. 31.

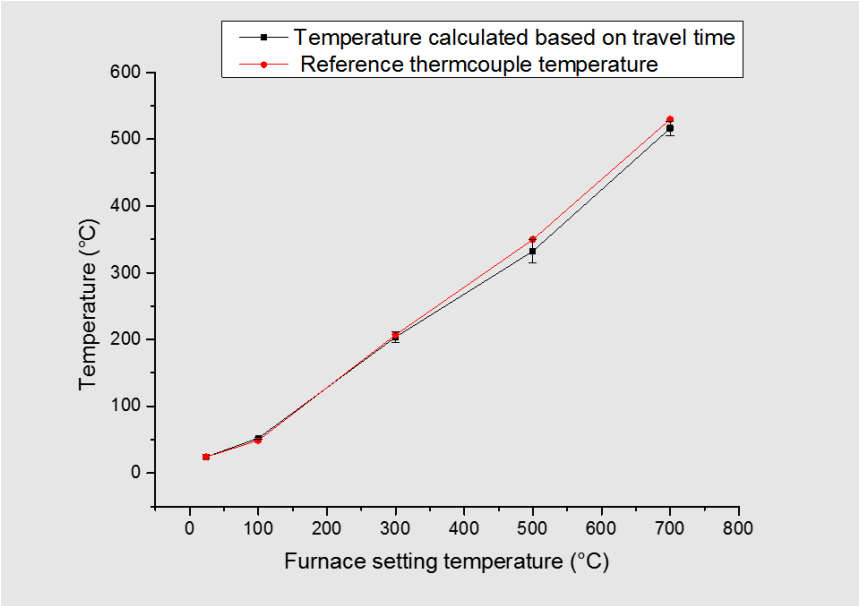

Fig. 31. Thermocouple reference temperature compared with temperature calculated based on travel time at the same furnace setting temperature.

3.4 Fiber optic sensing system III. (Milestone 8)

Fiber optic sensing system III is an all optical ultrasound system which the fiber optic ultrasound generator act as a signal generator and multiple FP receivers act as a signal receiver. A fiber optic sensing system III is shown in Fig.32. One generator and three receivers were used in this system.

Optical excitation generated ultrasound signals through a glass slide coated with a photoacoustic material, which was black PDMS in this case. The black PDMS set in between the supporting aluminum plate and the testing aluminum plate. An optical fiber, with a 1 mm core diameter, guided the light from a laser to the black PDMS. This system used three FP fiber sensors, named No.2, No.3 and No.4 FP fiber sensors. Three FP receiver IIs set on the same side of the signal generator. The distance between generator to FP fiber sensor No.2 (FP2), No.3 (FP3) and No.4 (FP4) was 4 cm, 3 cm, and 7.2 cm, respectively, as shown in Fig.33.

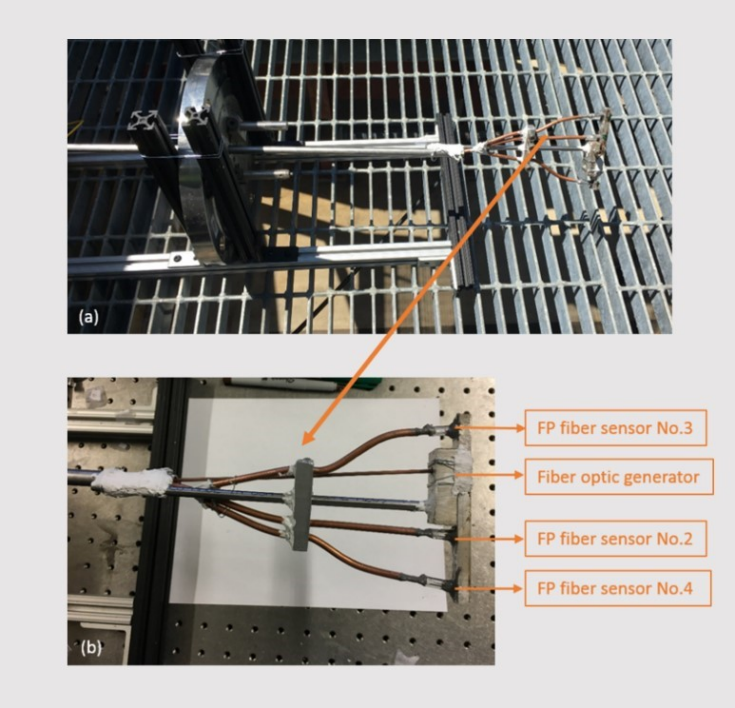

Fig.32. Fiber optic sensing system III

The system operation method is shown in Fig.33. We can rotate the central support pillar and move back and forward of the sensor head to obtain a 3D temperature measurement. There are 3 paths in one line, several lines in one plane, and several planes for the whole test. In Fig.33, it just shown 3 paths in one line and 2 lines in one plane, and just 1 plane.

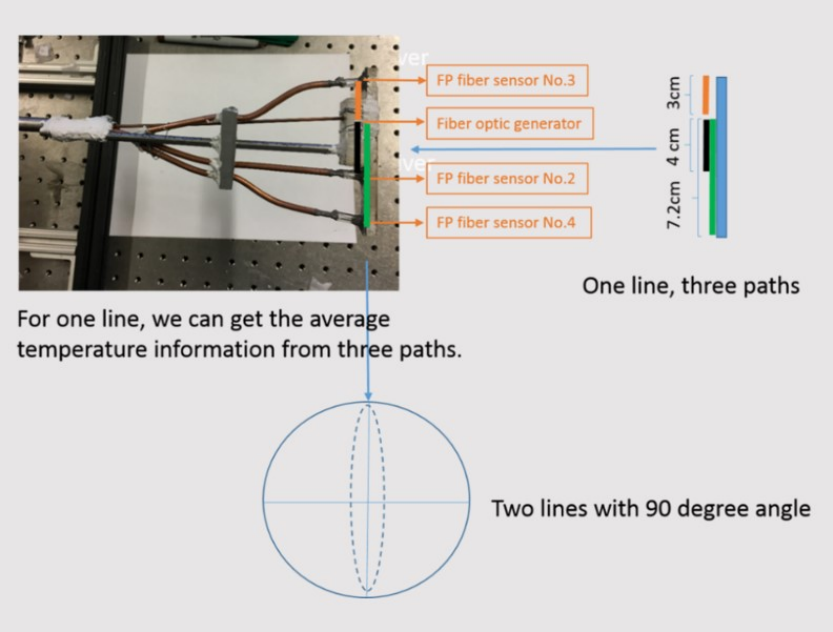

Fig. 33. System operation method.

3.5 Pilot test at GE Power. (Milestone 7 and Milestone 9)

3.5.1 Fiber optic sensing system I pilot test at GE ISBF.

This test was to test if the fiber optic sensing system I could be survived in boiler environment. This test was performed at the Industry Scale Burner Facility (ISBF) at GE's Clean Energy Center in Bloomfield, CT. The test location was chosen within an exhausting pipe of the ISBF as shown in Fig. 34. The temperature within the pipe is around 480 °F when the burner starts. The experimental setup is shown in Fig. 35. A fiber optic ultrasound generator was used as the signal generator, a PZT was used as the signal receiver. There was also a water cooling system in it. It can be seen clearly that the TOF of acoustic signals during the flame was fired was different compared with the ones obtained before and after the combustion event as shown in Fig. 36. The PZT receiver didn't survive a long time during the combustion event, it was broken after 10 minutes due to the high temperature. The fiber optic generator survived in the combustion events. This test shows that the traditional PZT receiver cannot survive in the high temperature environment, but the fiber optic sensors can.

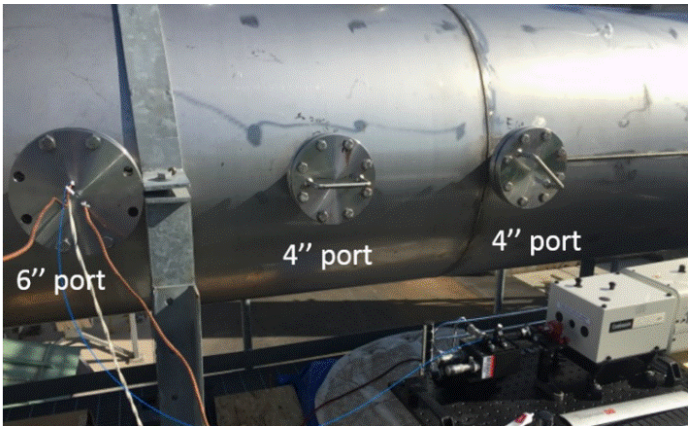

Fig. 34. Testing port on exhausting pipe of the ISBF

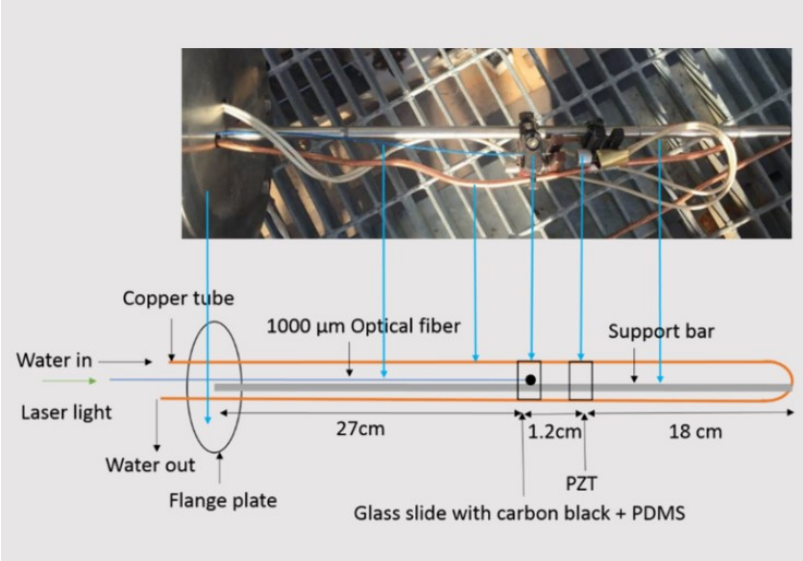

Fig. 35. Experimental setup for the Pilot Test Sensing System I.

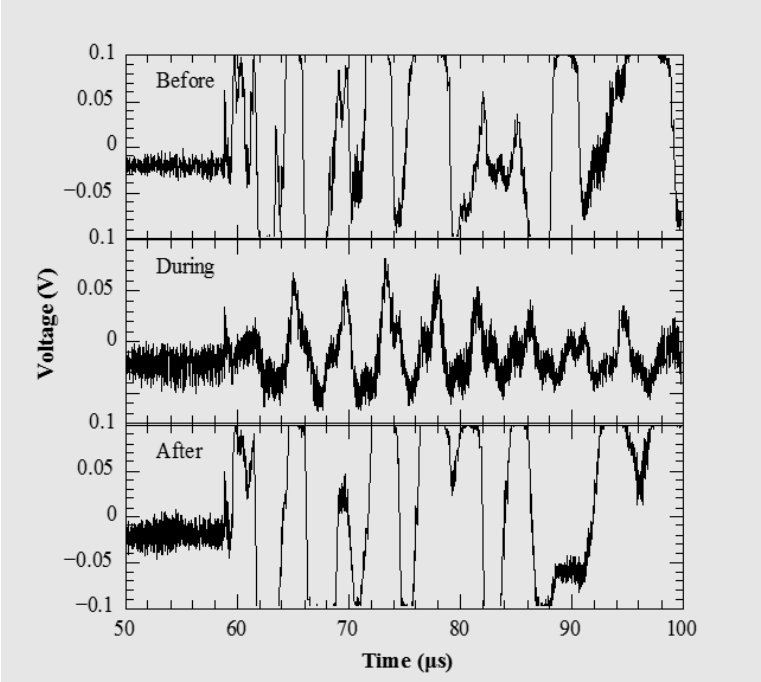

Fig. 36. TOF of acoustic signals during the flame, after flame and before flame.

The experimental measurement travel time information compared with GE's reference thermocouple temperature data are shown in Fig. 37. The y value are the total time measured by UML sensor, the x value are the reference temperature provided by GE ref. sensor. The relationship between reference temperature and the total time is linear which proves that the sound speed is directly proportional to the medium's temperature.

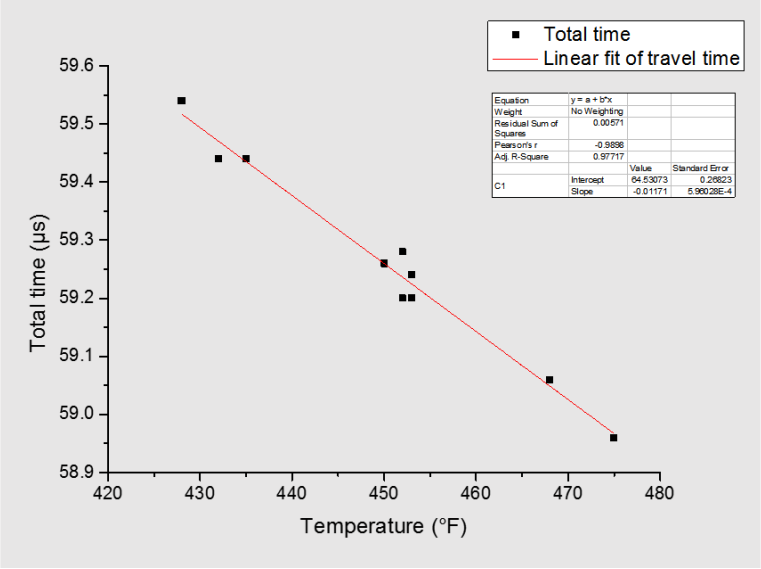

Fig. 37. Experimental measurement travel time compared with GE's reference temperature data.

The Fig. 38 shows the experimental measurement temperature compared with GE's reference thermocouple temperature data. The black points are the temperature information from GE Reference sensor. The red points are the temperature information calculated from UMass test sensor. The x value were the time frames. We started the temperature measurement from different time frames. We can found two data are matched.

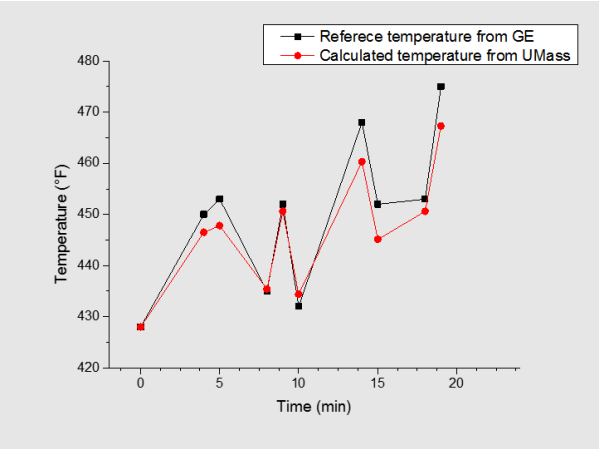

Fig. 38. Calculated temperature from our system compared with GE's reference temperature data.

3.5.2 Fiber optic sensing system II pilot test at GE's ISBF (Milestone 7)

The goal of this pilot test was to test the capability of using fiber optic sensing system II to detect the temperature change within an exhausting pipe. A fiber optic generator was used as a signal generator. An FP receiver I was used as a signal receiver. The test was performed on the exhausting pipe (Fig. 39) over the Industry Scale Burner Facility (ISBF) at GE's Clean Energy Center in Bloomfield, CT.

Our fiber optic sensing system II survived at least 2 hours during the long time sustained combustion. In this 2 hours, we got very clearly ultrasound signal. We got at least 20 data. The temperature range of this test was from 285 °o to 320 °t recorded by our reference thermocouple. The generator broke after 2 hours sustained combustion, the receiver was still workable after 3 hours test. The generator broke because of the 1000 μm fiber broke at the fixing bolt area. The photoacoustic material was still workable after 22 hours long time sustained combustion. The receiver was not workable after 22 hours long time sustained combustion.

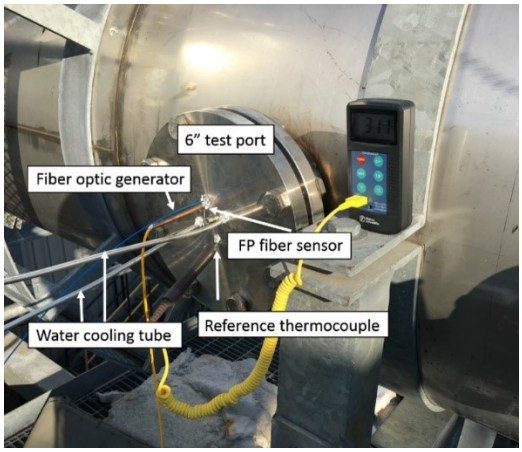

Fig. 39. Test location.

The experimental setup is shown in Fig. 40 and Fig. 41. Ultrasound signals were generated by optically excited on a glass slide coated with a photoacoustic material, which is black PDMS in this case. An optical fiber with 1 mm as the core diameter was used to guide the laser to the glass slide. An FP receiver I was

used as the signal receiver. Two aluminum tube was used for water cooling system. A copper tube was used for fiber protection. A 6'' flange was used to mount the system onto the 6'' port of the pipe. The distance between generation and receiver part was 12.7 mm. The distance between generation and flange was 30 cm. The spectrums of the FP fiber receiver in different temperature was shown in Fig. 42. The wavelength was chosen at 1536 nm.

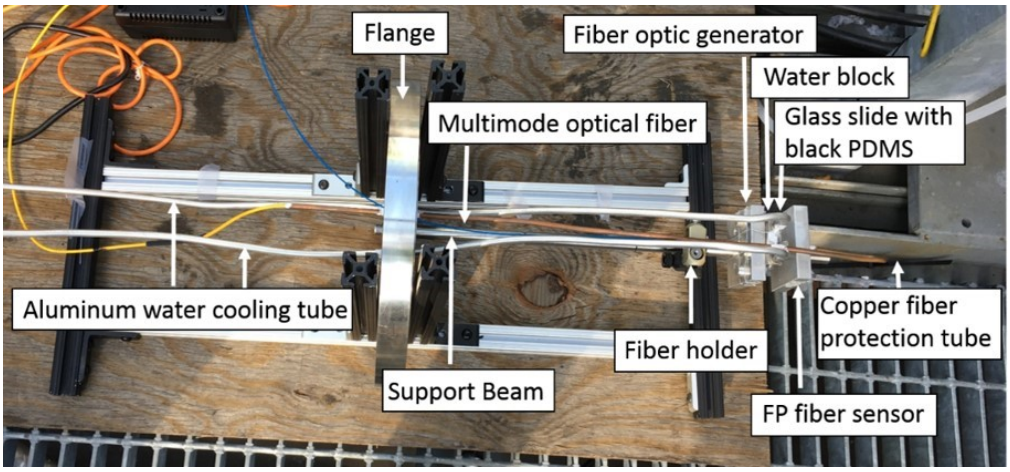

Fig. 40. Experimental setup of optical sensing system (photo).

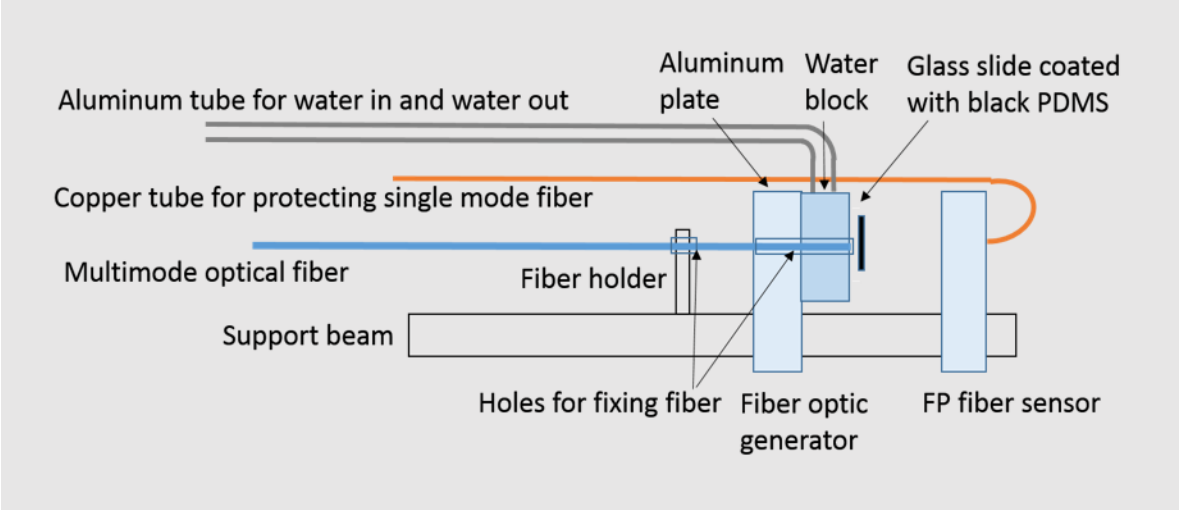

Fig. 41. Experimental setup of optical sensing system (Structure).

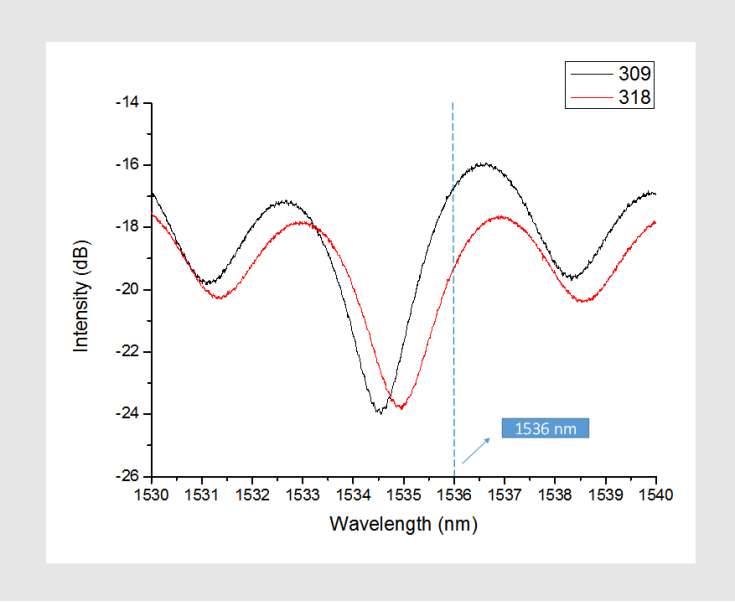

Fig. 42. Spectrum of FP fiber receiver at different temperature.

We got at least 20 data at the different temperature. Several typical ultrasound signals were shown in Fig. 43. The temperature information was recorded by reference thermocouple. The relationship of the temperature data and the travel time information was shown in Table 5. It had also been plotted in Fig. 44.

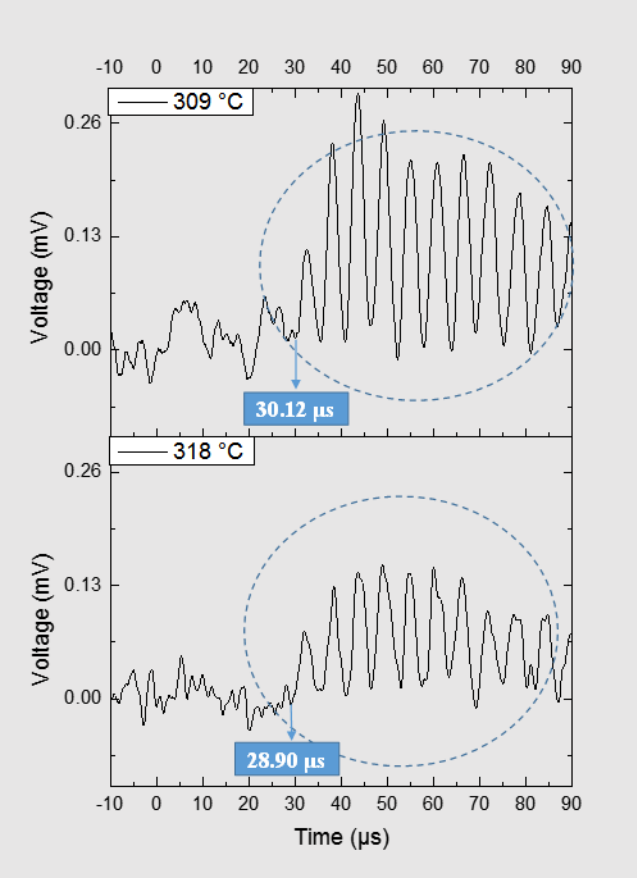

Fig. 43. Acoustic waves at different temperature.

Table 5. The relationship between thermocouple temperature and the ultrasound travel time

Reference thermocouple temperature (ºC)	Trial	Travel time (µs)
285	1	33.68
285	2	33.70
298	1	31.74
303	1	30.94
304	1	30.84
306	1	30.50
308	1	30.20
309	1	30.12
311	1	29.76
312	1	29.38
312	2	29.66
314	1	29.38
314	2	29.44
315	1	29.26
315	2	29.20
316	1	29.26
318	1	28.90
318	2	28.78
319	1	28.66
319	2	28.42
320	1	28.46

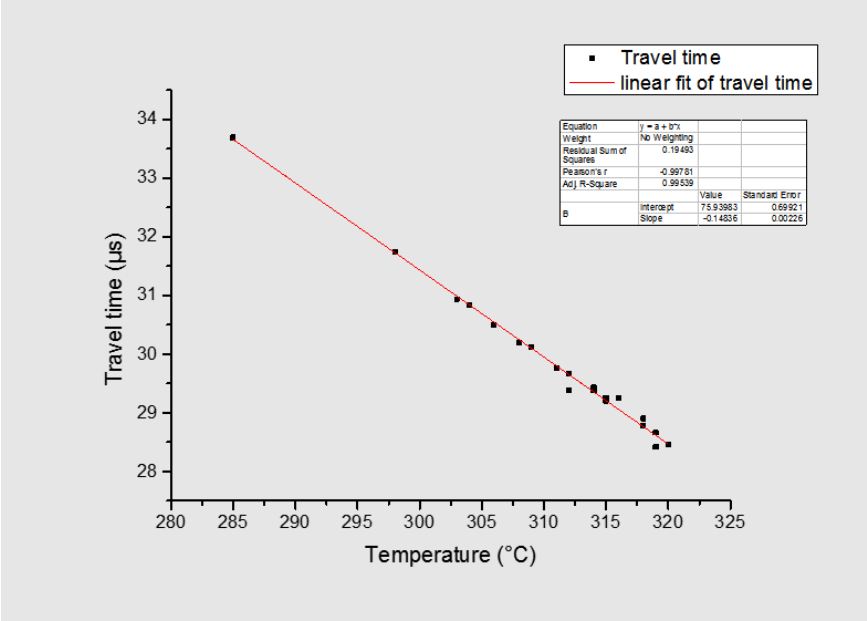

Fig. 44. Experimental measurement travel time compared with our reference temperature data.

The relationship between thermocouple temperature and the ultrasound travel time is linear which proves that the sound speed is directly proportional to the medium's temperature.

The Fig. 45 shows the experimental measurement temperature compared with our reference thermocouple temperature data. The black points are the temperature information from Reference sensor. The red points are the temperature information calculated by UML sensing system. The x value were the time frames. We started the temperature measurement from different time frames. The biggest variation is 7.86 °C, the percentage over the measurement is 2.49%. The small difference between these two data caused by the temperature variation, the calculated temperature was the average temperature between the generator and the receiver, the reference temperature was only the point near generator location.

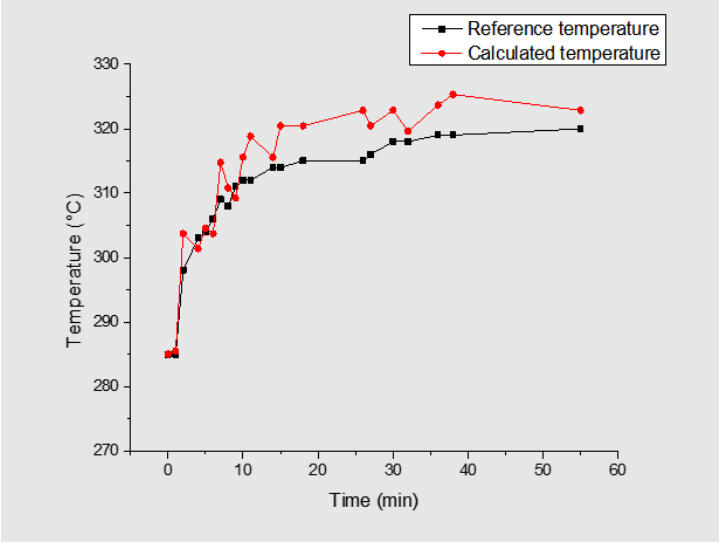

Fig. 45. Calculated temperature from our system compared with our reference temperature data.

Our fiber optic sensing system II survived at least 2 hours during the long hour sustained combustion. In this 2 hours, clearly ultrasound signals were recorded by our optical sensing system.

The fiber optic generator was survived for 2 hours in sustained combustion. The 1000 μm optical fiber broke at the screw fix area after 2 hours combustion. The photoacoustic material (Black PDMS) survived 22 hours sustained combustion until the test end.

The FP receiver was survived at least 3 hours in sustained combustion. The spectrum shift with the temperature increase. The FP fiber receiver I broke after 22 hours sustained combustion because the single mode fiber coating area was made of the polymer, which cannot be survived in such long time. The water cooling system on the generator part could also be used after 22 hours sustained combustion. The relationship between thermocouple temperature and the ultrasound travel time was linear which proves our assumption.

3.5.3 Fiber optic sensing system III pilot test at ISBF. (Milestone 9)

1) Fiber optic sensing system III pilot test 1 (05/2018)

This was a cold flow test on ISBF. There was no combustion in this pilot test but the sensing head was impacted by air flow in the pipeline. Opening the exhaust fan of the ISBF introduced strong air flows. First, we recorded data in the no wind condition. Second, we recorded data in the wind condition. Last, we rotated the testing system 90 degrees and obtained other data in the wind condition, to perform a 2D temperature reconstruction. Our sensing system was still in good condition after the test.

The test location was within an exhaust pipe of the ISBF. One 6'' port was used for this test as shown in Fig. 46. Our sensing systems could conveniently use this port.

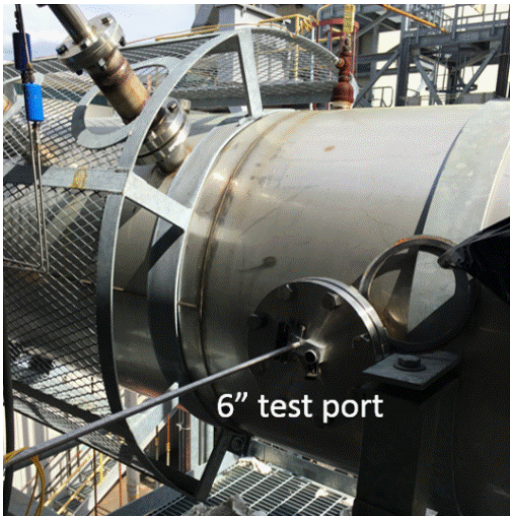

Fig. 46. Test location.

Fig. 47 and Fig. 48 show the experimental setup. Optical excitation from the fiber optic ultrasound generator, produced ultrasound signals through a glass slide coated with a photoacoustic material, which was black PDMS in this case. The black PDMS was placed between the supporting aluminum plate and the testing aluminum plate. An optical fiber, with a 1 mm core diameter, guided the light from the laser to the black

PDMS. This system used three FP receiver IIs, named FP2, FP3 and FP4. Three FP receiver IIs was set on the same side of the signal generator. The distance between generator to FP receiver II No.2 (FP2), No.3 (FP3) and No.4 (FP4) was 4 cm, 3 cm, and 7.2 cm, respectively, as shown in Fig. 49. A tunable laser (TLB-6600, Venturi TM Tunable Laser) acted as a light source to excite the FP fiber sensors through a circulator. A photodetector (PDA10C, Thorlabs) detected the reflected light through the circulator as well as converted the optical signal into electrical signal. The spectrum of FP fiber sensors manifested in Fig. 50. The wavelength of tunable laser was set at 1560 nm. The FP sensors had different cavity lengths, therefore their spectra were different.

Each FP sensor receiver comprised of one data path. During the test, the three FP sensor receivers recorded data along one line, with and without air flows. Furthermore, the testing line rotated 90 degrees, and another three data paths (one line data) were recorded in the cold flow test condition.

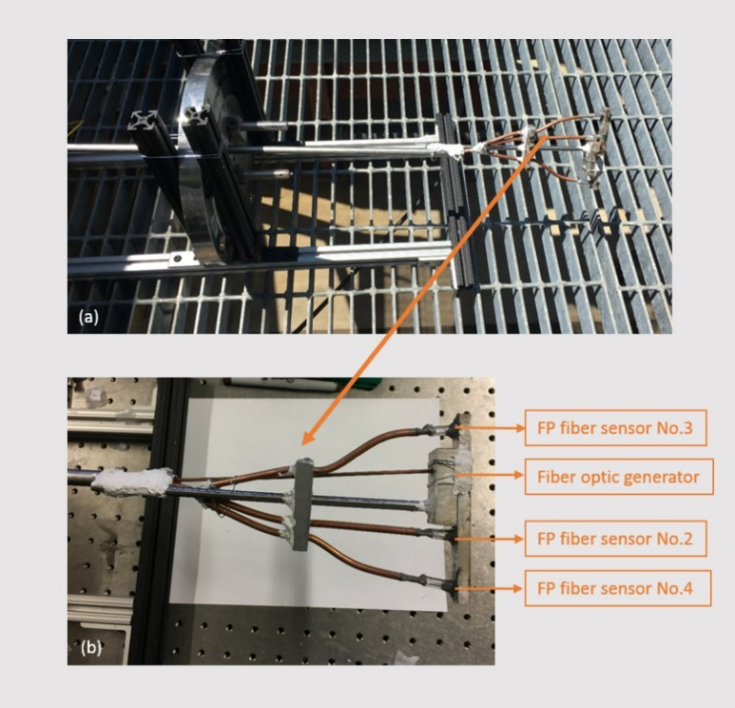

Fig. 47. Experimental setup of UML optical sensing system.

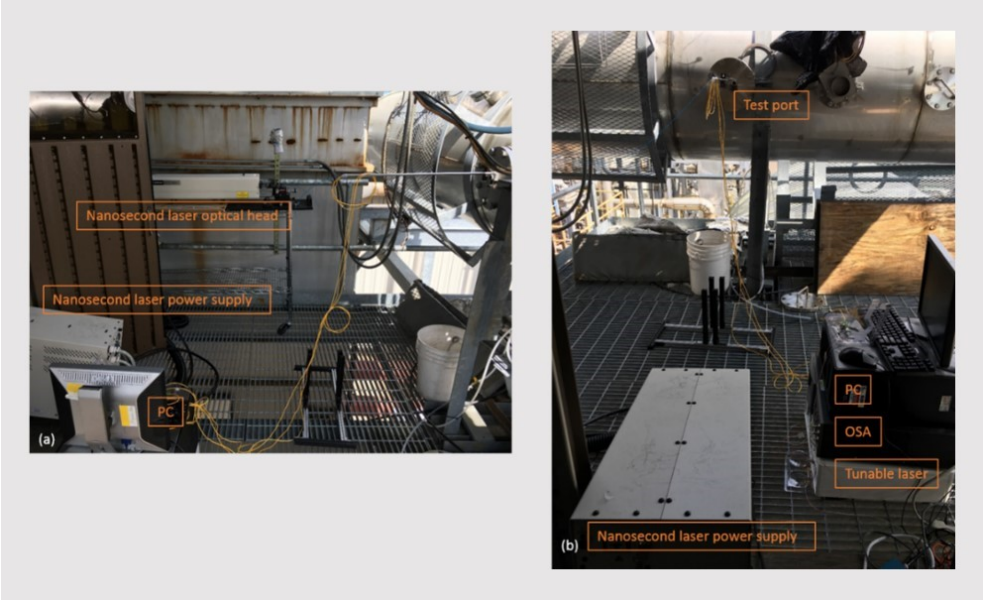

Fig. 48. Experimental setup of optical sensor system (Equipment).

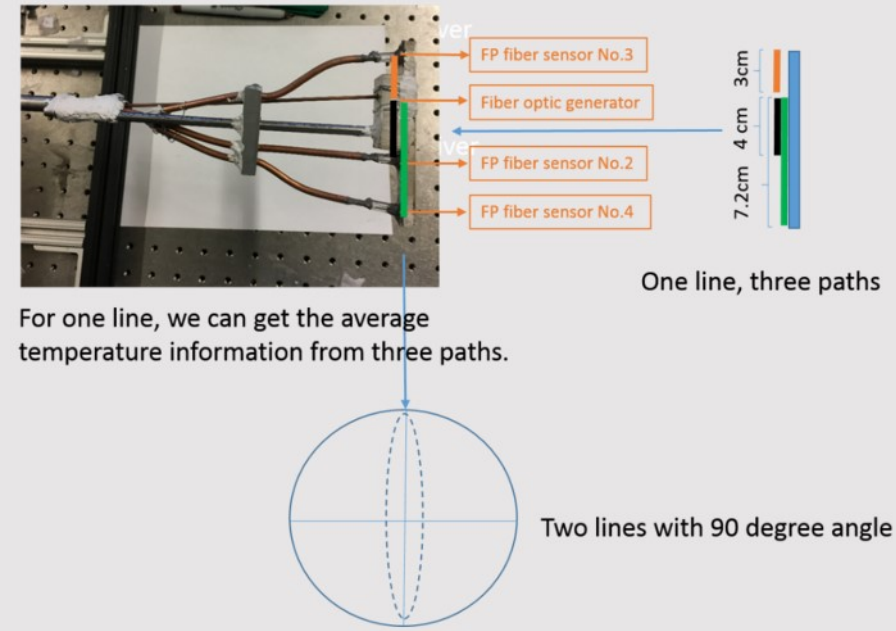

Fig. 49. System operation method.

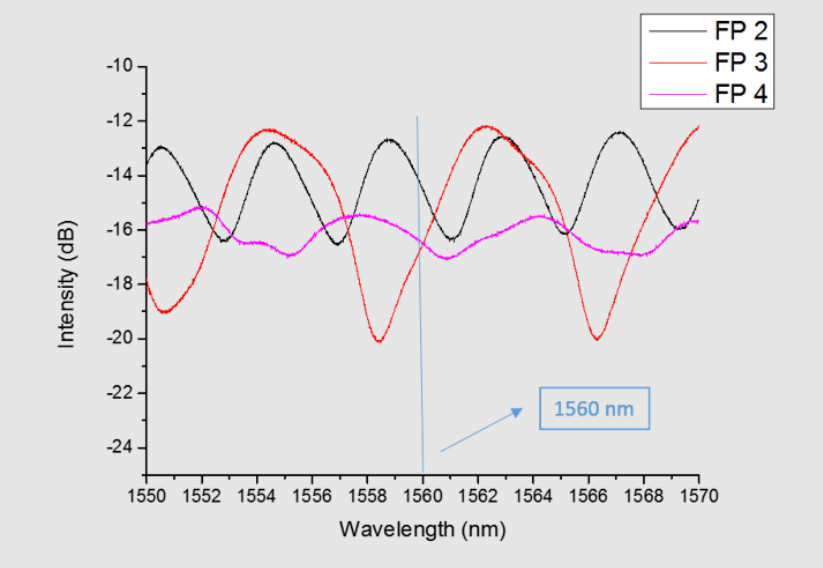

Fig. 50. Three FP fiber sensor spectrum.

Fiber optic sensing system III survived the test. Ultrasound signals successfully detected different conditions. The ultrasound signals that the different receivers detected in the cold flow test condition are shown in Fig. 51, Fig. 52 and Fig. 53 and Table 6.

As shown in Fig. 54, the detected ultrasound travel time FP2 detected was 14.12 µs. Since the distance from FP2 to the generator was 4 cm, the sound speed was approximately 2832 m/s. As shown in Fig. 53, we found the ultrasound travel time FP3 detected was 10.40 µs. Since the distance from FP3 to the generator was 3 cm, the sound speed was approximately 2884 m/s. As shown in Fig. 54, we found the ultrasound travel time FP4 detected was 25.16 µs. Since the distance from FP4 to the generator was 7.2 cm, the sound speed was approximately 2863 m/s.

Since we know the sound speed (Surface Acoustic Wave) travel in aluminum plate is approximately 2800 m/s, we expect it is an ultrasound signal. Since the Fiber optic generator and the FP fiber sensors were in the same side, we expect the ultrasound signal detected would be a surface acoustic wave.

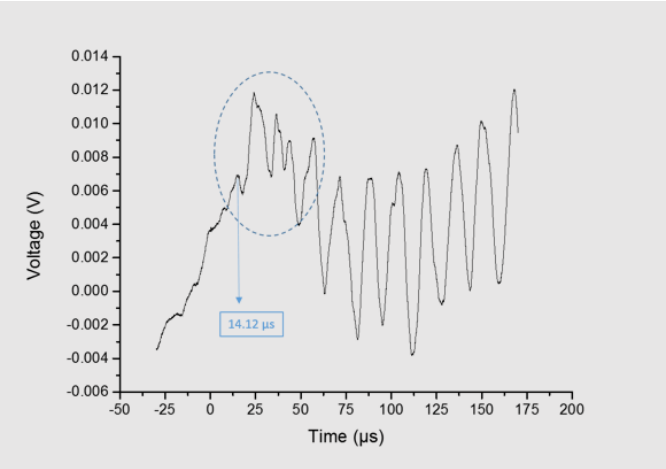

Fig. 51. FP2 in the wind condition.

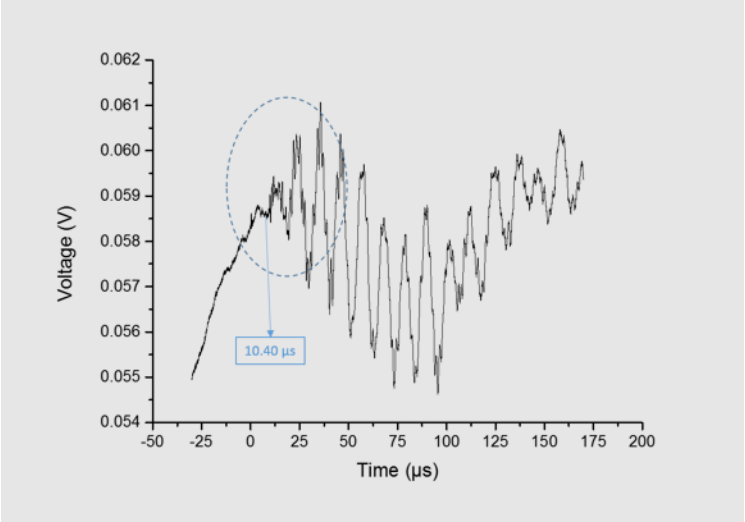

Fig. 52. FP3 in cold flow test condition.

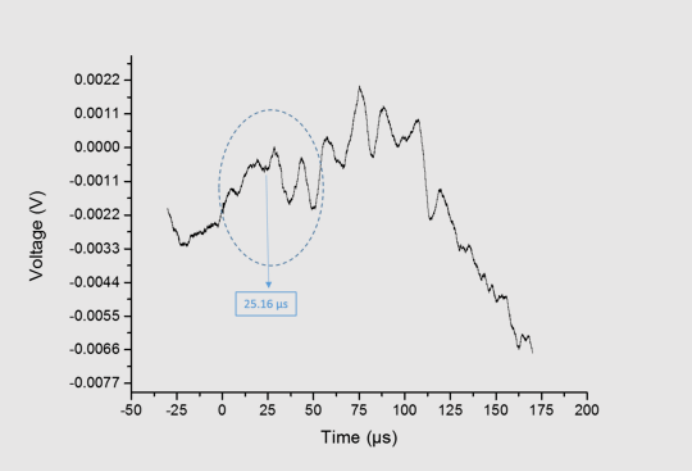

Fig. 53. FP4 in cold flow test condition.

Table 6. The ultrasound travel time on different condition.

FP2	No wind	14.04
	Air flow	14.12
	Air flow (Rotate 90 degrees)	14.22
FP3	No air flow	10.18
	Air flow	10.14
	Air flow(Rotate 90 degrees)	10.20
FP4	No air flow	25.10
	Air flow	25.16
	Air flow (Rotate 90 degrees)	25.26

2) Fiber optic sensing system III pilot test 2 (06/2018)

The aim of this test was to examine the ability of fiber optic sensing system III to measure the temperature distribution inside an exhaust pipe. Similar setup as previous fiber optic sensing system III pilot test 1 was deployed. A 1 mm multimode fiber optic based on photoacoustic principle was used to generate ultrasound signals, and three Fabry–Perot (FP) sensors made of single mode fibers used to receive these signals. Measuring the time of flight of the ultrasound signals facilitates temperature acquisition, because the speed of ultrasound is directly proportional to the temperature of the propagation medium.

The test was performed in an exhaust pipe of the Industry Scale Burner Facility (ISBF), at GE's Clean Energy Center in Bloomfield, CT. We tested the system in open-air environment and the data was obtained from two sensors at room temperature. However, the system failed to obtain signals when inserted into the pipe due to the excessive air flow. Finally, after combustion, when the temperature inside the pipe increased to 170 °C, we still did not obtain a signal.

The test was conducted within an exhaust pipe of the ISBF, as shown in Fig. 55.

The system was inserted into the pipe through a 6''dia port. Fig. 54 shows the port before and after the system was inserted. Fig. 55 shows the structure of the system.

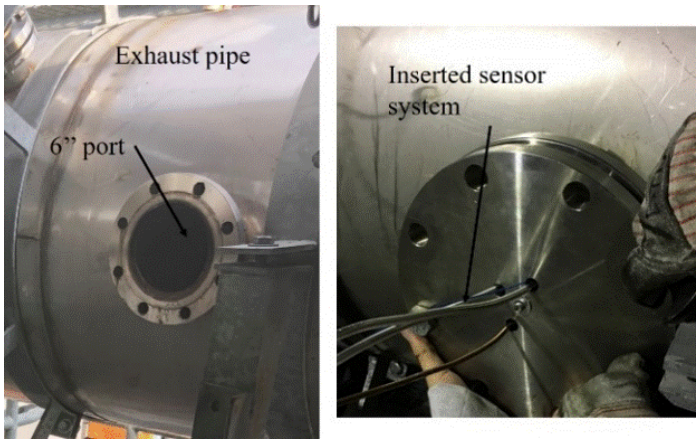

Fig. 54. The system inserted into the pipe through a port.

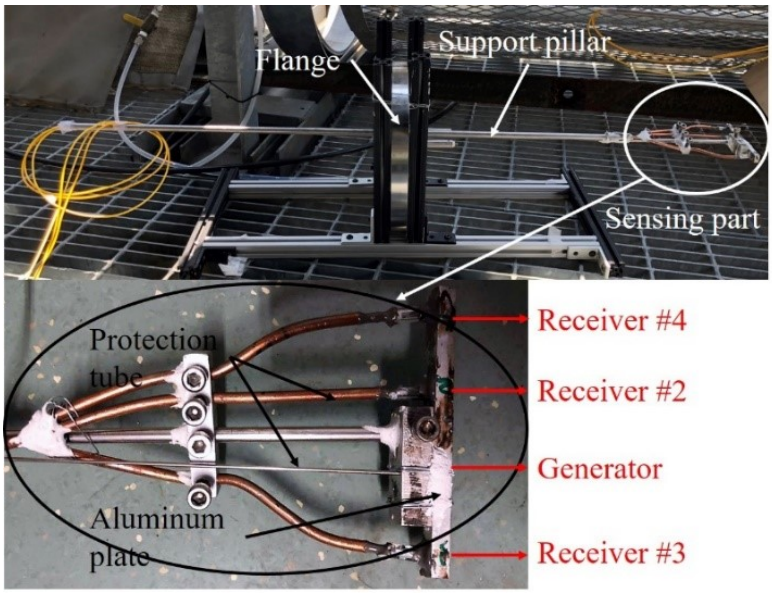

Fig. 55. The structure of the sensing system.

Aluminum tubes that were fixed on an aluminum plate, protected all the three receivers along with the generator. When laser pulses hit the photoacoustic material, which was black PDMS in this project, ultrasound signals were generated and then propagated inside the aluminum plate and reached three sensors. The distance from the generator to the receiver #2, #3, #4 was 4 cm, 3 cm, and 7.2 cm, respectively. When the temperature changed, the speed of ultrasound in the aluminum plate also changed, thus the ultrasound signals' time-of-flight changed accordingly.

We tested the system's ability of generating and receiving ultrasound signals in open-air environment first. The spectra of three sensors are shown in Fig. 56.

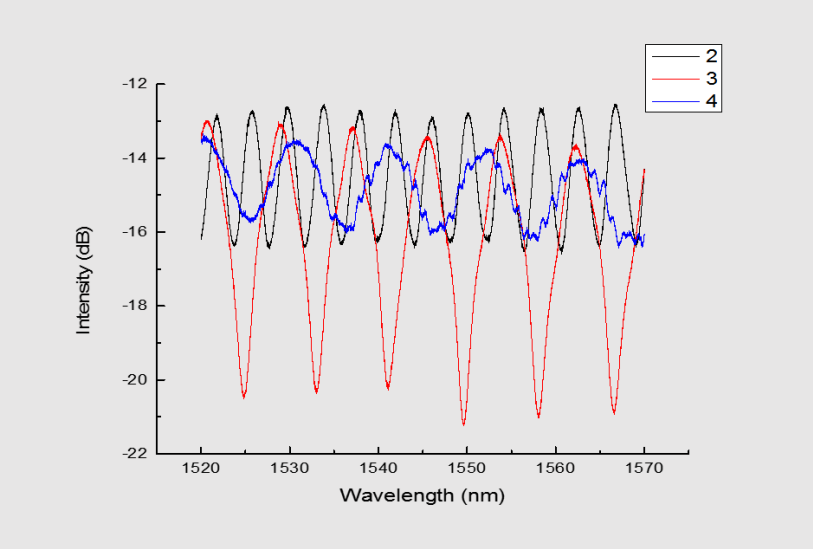

Fig. 56. The spectrum of three sensors in open air.

As it can be seen from Fig. 57, the spectrum of sensor #4 is not as accurate as #2 and #3. In the open-air experiment, only #2 and #3 sensors detected ultrasound signals. Fig. 59 shows the signals and their time of flight. The signals cannot be identified distinctly because of excessive noise, and inaccurate time of flight.

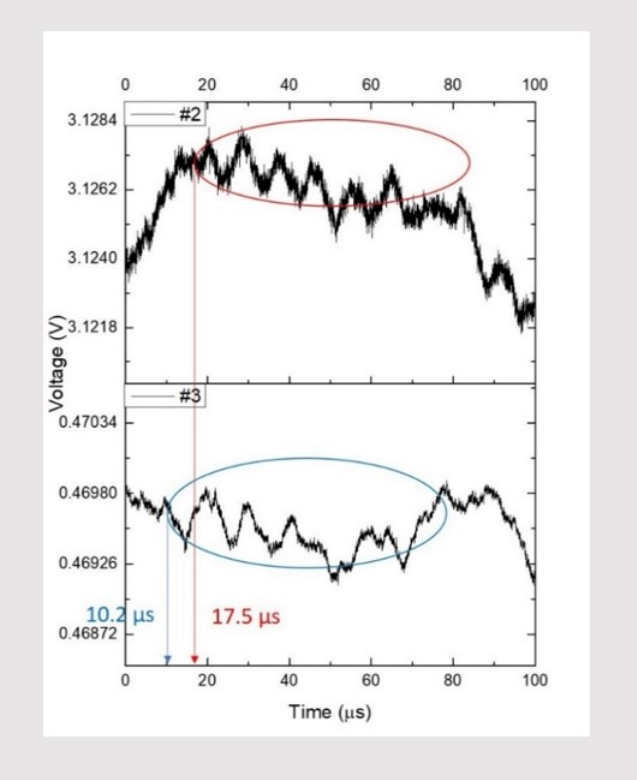

Fig. 57. The ultrasound signals detected by the sensor #2 and #3 in open air.

The actual distance from the generator to the sensor #2 and #3 is 4 cm and 3 cm. The ultrasound speed is $\frac{0.04\ \mathrm{m}}{17.5\ \mu\mathrm{s}} = 2286\frac{\mathrm{m}}{\mathrm{s}}$ from #2 and $\frac{0.03\ \mathrm{m}}{10.2\ \mu\mathrm{s}} = 2941\frac{\mathrm{m}}{\mathrm{s}}$ from #3, respectively. The literature value of ultrasound speed in aluminum in room temperature is approximately 3080 m/s.

After the system sat in the pipe, the sensors' spectra became very unstable and shifted quickly due to air flow. We failed to detect signals inside the pipe. We checked the system after taking it out of the pipe. The glue that used to mount the sensors was crumbling. Next time, a stickier glue will apply.

The entire system worked well in the open-air environment, but it failed in the exhaust pipe. A glue that is stickier and more durable must reinforce the system, especially the joints of sensors. A portable and simply-equipped one is eagerly needed.

3) Fiber optic sensing system III pilot test 3 (02/2019)

The aim of this pilot test is to test the capability of using the fiber optic sensing system III to reconstruct the temperature distribution within an exhaust pipe. Similar setup as previous fiber optic sensing system III pilot test 2.

Problems encountered from the previous pilot test (06/2018): 1) The FP fiber sensors' spectra were unstable and shifted quickly during the pilot test. The glue that was used to mount the FP fiber sensors melted at high temperature at 170°C. 2) The nanosecond laser (Surelite-I-10, Continuum) had problems, the laser water cooling system and the coupling system were dysfunctional.

The new pilot test (02/2019) solved the above issues: 1) We used a new durable glue ("Technicqll" high temperature glue) for FP fiber sensors fabrication. The glue that was used to mount the FP fiber sensors endured high temperature. FP fiber sensors' spectra were stable during the pilot test. All three FP fiber

sensors detected stable signals. 2) We used a new portable nanosecond laser (LPS-A-1064, Cnilaser) for the pilot test. It was easy to install during the pilot test.

There were several ignitions during this pilot test. The testing area temperature ranged from 300 ^{o}h to 500 ^{o}t. The test lasted for 3 hours. Before the pilot test, the ultrasound sensing system was tested in the lab, the test results proved that our sensing system was able to detect the ultrasound signal at room temperature environment. During the pilot test, the three FP fiber sensors detected stable spectra.

However, our new nanosecond laser had problems, the trigger signal could not be detected by the DAQ card, the trigger signal was not stable. The ns laser was returned to the manufacturer for repair on 01/2019. the ultrasound signal was not detected during the pilot test. We planned to have a pilot test on 01/2019, because of the nanosecond laser problem, we missed the 01/2019 pilot test.

Fig. 58 and Fig. 59 show the experimental setup. As shown in Fig. 58, a fiber optic (ultrasound) generator acted as the signal generator. Optical excitation generated ultrasound signals through a glass slide coated with a photoacoustic material, which was black PDMS in this case. The black PDMS is set in between the supporting aluminum plate and the testing aluminum plate. An optical fiber, with 1 mm core diameter, guided the light from a nanosecond laser (LPS-A-1064, Cnilaser) to the black PDMS. Three FP fiber sensors were used in the system. These were named No.1, No.2 and No.3 FP fiber sensors. Three FP fiber sensors was set on the same side of the signal generator. A durable glue ("Technicqll" high temperature glue) was used to build the FP fiber sensor receiver part. The glue could survive up to 1200°C temperature. All receivers and generator were protected by tubes and are fixed on an aluminum plate. When laser pulses hit the photoacoustic material, which is black PDMS in this project, ultrasound signals are generated and then propagate inside the aluminum plate, and reach three sensors. The distance from the generator to the receiver No.1, No.2, No.3 was 7.2 cm, 4 cm, and 3 cm, respectively. A tunable laser (TLB-6600, Venturi TM Tunable Laser) acted as a light source to excite the FP fiber sensors through a circulator. A photodetector (PDA10C, Thorlabs) detected both the reflected light through the circulator as well as converted the optical signal into electrical signal. The spectra of FP fiber sensors manifested in Fig. 60. In order to magnify the output, we intended to select the "Q-point" at the center of the "linear range" where the slope was the highest. In this case, 1527.7 nm was selected. The photodetector was set at 30 dB. The output power of the tunable laser was 7.60 mW. When the laser source released a pulsed signal, a trigger signal was sent from the laser system to trigger a data acquisition card (DAQ) (M2i.4032, Spectrum) at a sampling rate of 50 MHz.

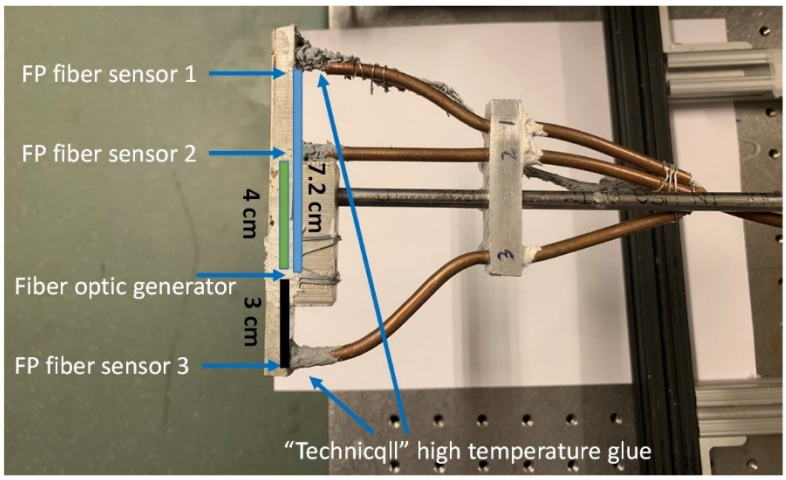

Fig. 58. Experimental setup of UML optical sensing system (Sensor)

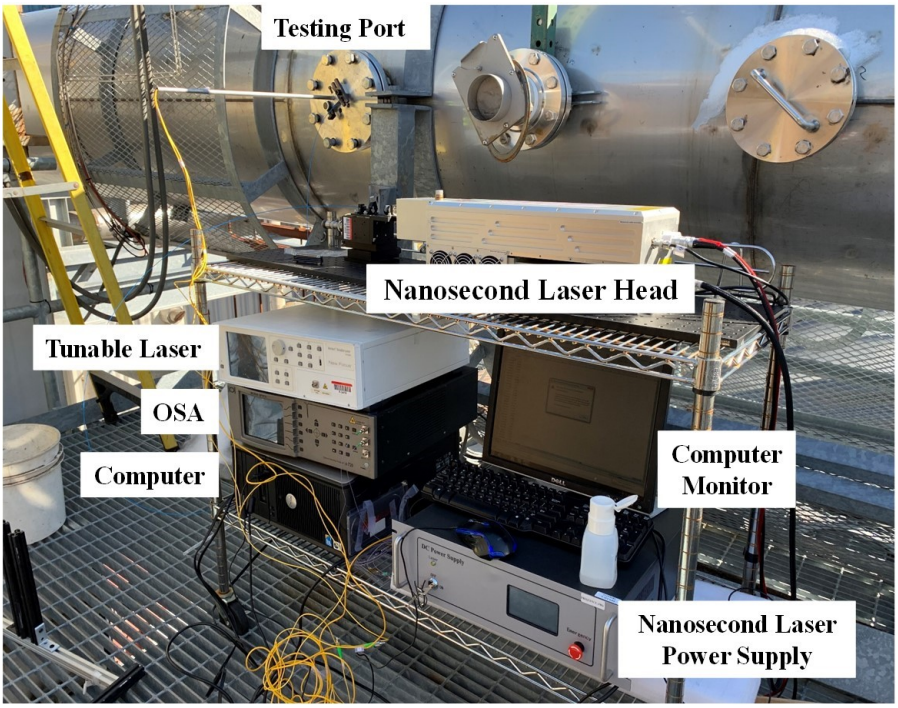

Figure 59. Experimental setup of optical sensing system and data acquisition system (Equipment)

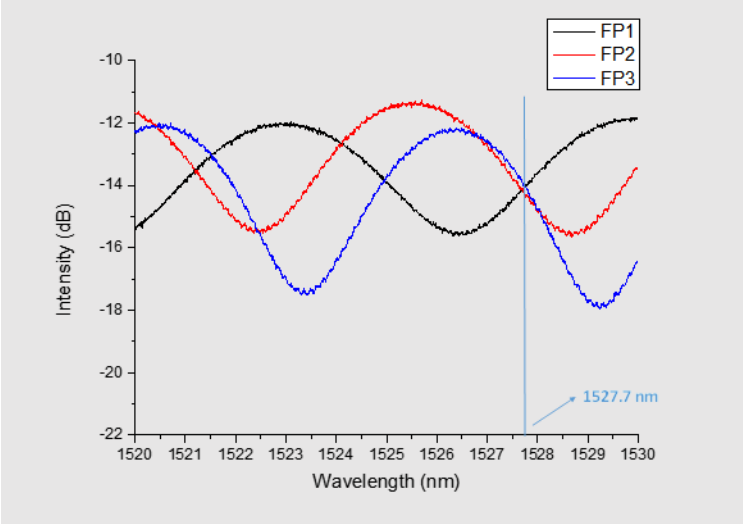

Fig. 60. The spectra of three sensors in open air environment (2°C).

All three FP fiber sensors survived under high temperature. The spectra of these three FP fiber sensors in open air environment (2°C) and boiler environment (320°C) were recorded and is shown in Fig. 61.

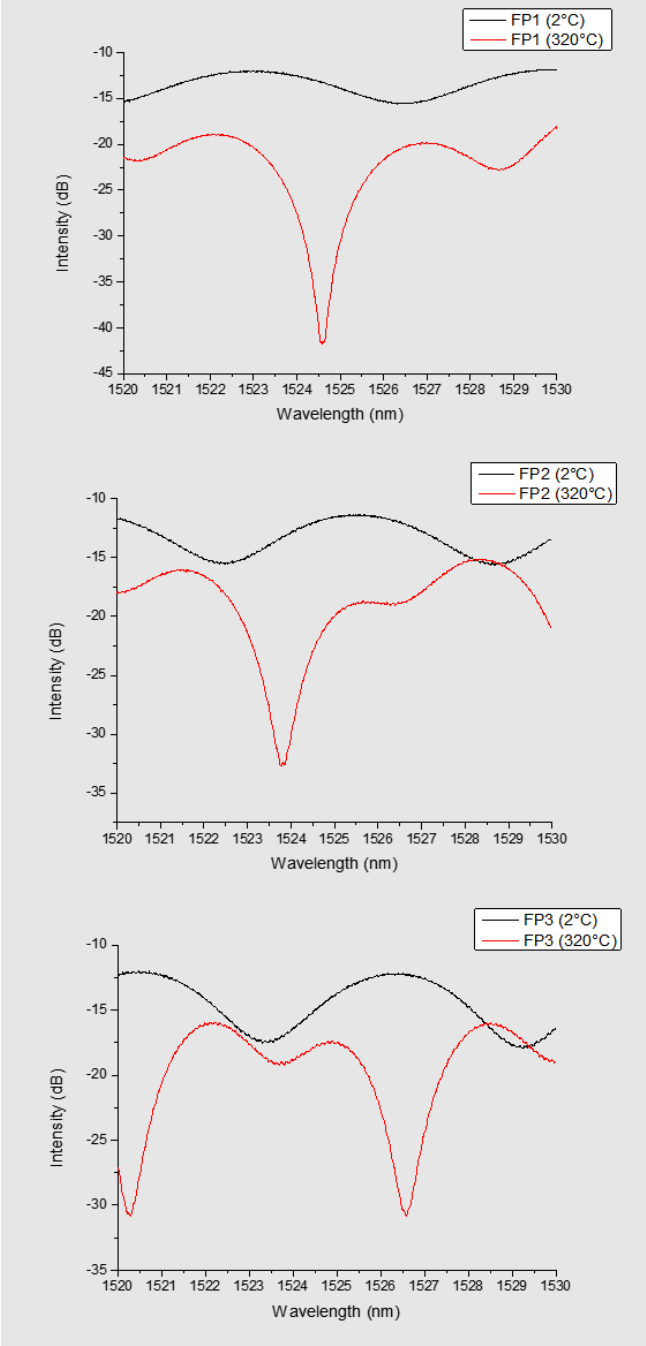

Fig. 61. The spectra of three sensors in open air (2°C) and in boiler (320°C).

Before the pilot test, we did a test in the lab environment (22°C). In the lab experiment, all three sensors had successfully detected the ultrasound signals. Fig. 62, Fig. 63 and Fig. 64 show the signals and their time of flight.

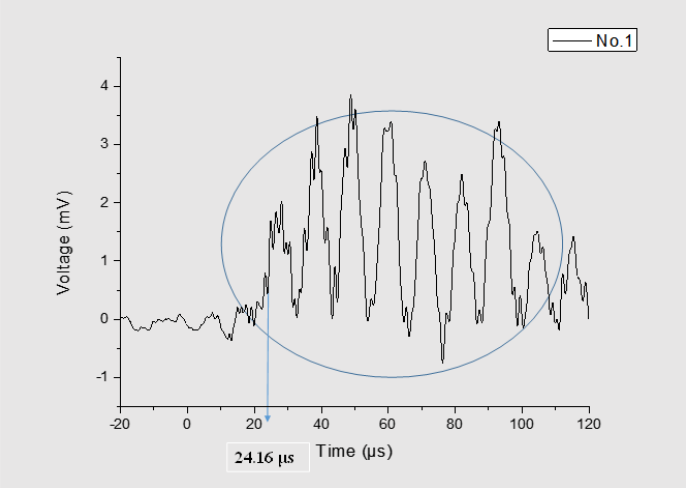

Fig. 62. The ultrasound signal detected by FP1 receiver (22°C).

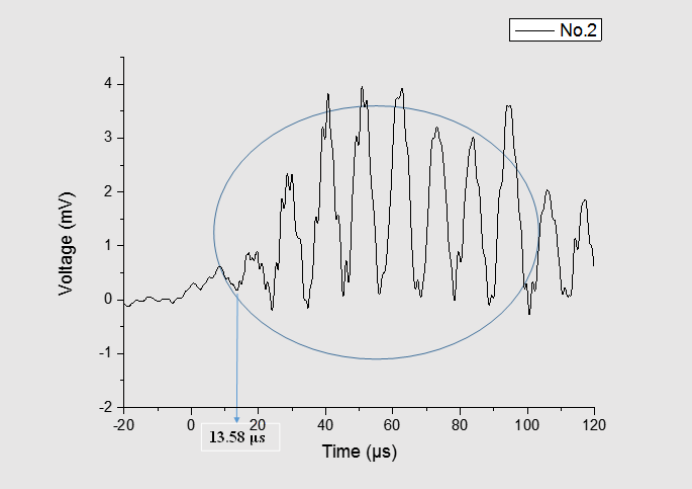

Fig. 63. The ultrasound signal detected by FP2 receiver (22°C).

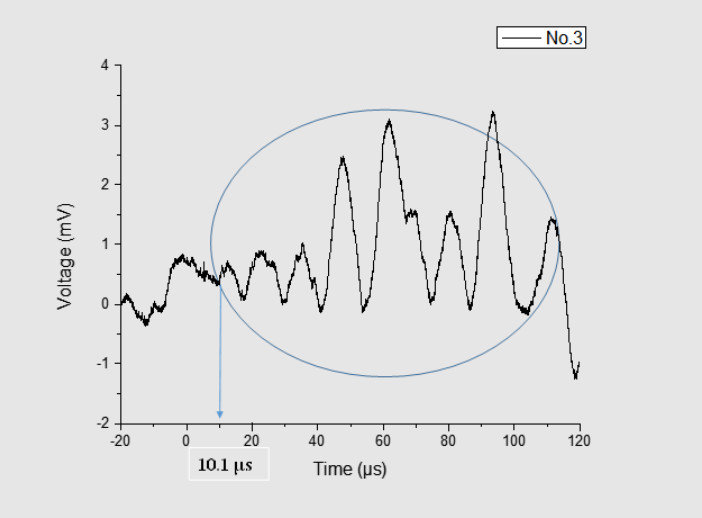

Fig. 64. The ultrasound signal detected by FP3 receiver (22°C).

As shown in Fig. 62, the detected ultrasound travel time of FP fiber sensor No.1 was 24.16 μs. Since the distance from FP1 to the generator was 7.2 cm, the speed of sound was approximately 2980.13 m/s. As shown in Fig. 63, we found the detected ultrasound travel time of FP fiber sensor No.2 was 13.58 μs. Since the distance from FP2 to the generator was 4 cm, the sound speed was approximately 2945.50 m/s. As shown in Fig. 64, we found the ultrasound travel time FP fiber sensor No.3 detected was 10.10 μs. Since the distance from FP3 to the generator was 3 cm, the sound speed was approximately 2970.29 m/s.

Since the speed of sound (Surface Acoustic Wave travel) in aluminum plate was 3040 m/s, hence we concluded that the detected signal was an ultrasound signal. The Fiber optic generator and the FP fiber sensors were along the same plane of the aluminum plate, therefore the received ultrasound signal was concluded to be a surface acoustic wave.

During the pilot test, our ultrasound detection system did not work successfully. The laser equipment had problems. The trigger signal from the nanosecond laser was not stable, and the system did not detect ultrasound signal. From the spectra in Fig. 66, we found our sensors were good during the combustion process. But since there were problems with the equipment, we couldn't detect any ultrasound signal. Fig. 65 shows the system after the combustion test. The sensing system head structure was still intact. The glue that used to mount the FP fiber sensors did not melt. Three FP fiber sensor cables were broken in the protection tube when we pulled out the sensing system head from the testing port, because the combustion had burned the fiber cables making it fragile.

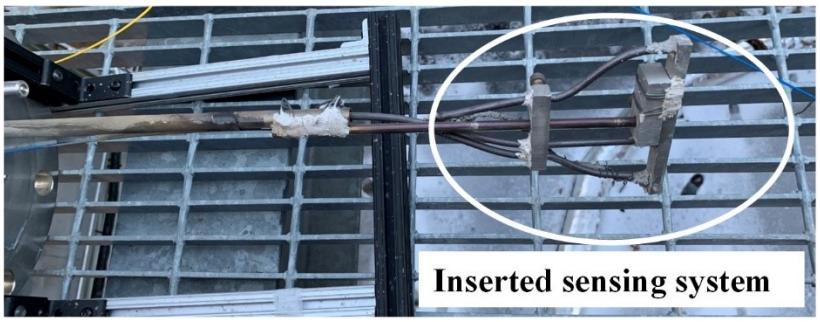

Fig. 65. The sensor head part after pilot test.

All three FP fiber sensors fabricated in UML Optics laboratory, survived the combustion process during the pilot test at the Industry Scale Burner Facility (ISBF) at GE's Clean Energy Center in Bloomfield, CT. The proposed optical part of the sensing system was able to acquire data at high temperature of 320°C. The sensor has shown good spectrum response under harsh conditions presented in the exhaust pipe. The proposed ultrasound part of the sensing system was tested in the lab premises and the result is analogous with the general acquired truth of the speed of sound wave travelling in Aluminum. The lab test result showed that our optical ultrasound sensing system could be used to detect the ultrasound signal at room temperature. However, at higher temperatures of 320°C the system did not show any response. This failure, we believe is due to the defective functioning of the nanosecond laser. The sensor head structure was still intact after the combustion test. Ultrasound signal was not detected during the pilot test.

3.6 Code-division multiplexing

For real time temperature field construction, the sampling rate needs to be fast enough to catch the field variation. Hence, simultaneous emission and receiving are desired which introduces cross-talking. Acoustic multiplexing is a challenging task especially when the signal is weak and environment is noisy. Compared to acoustic waves, radio and electromagnetic waves attracted attention in the past. There exists a significant amount of research for both multiplexing and SNR enhancement in regards to radio waves. There are three major approaches, which can realize signal multiplexing: time, frequency, or code divisions. Among them, the technology of Code-division multiple access (CDMA) is well studied which could allow parallel multiplexing, even if signals overlap in time or frequencies. Moreover, it has been known that extending the length of signal significantly improves SNR. For acoustic signals, these multiplexing techniques have also been widely used, mainly for sonar and acoustic communications. The CDMA modulation technique has been proposed and studied to guarantee high network throughput, low channel access delay and low energy consumption.

1) CDMA-based acoustic sensor system

Analogous to underwater communication, CDMA is proposed as the multiplexing scheme for the measurement of transition time of acoustic waves because it is robust to multipath and frequency selective fading effects. In addition, SNR can be increased by extending code length. Each emitter is assigned a unique pseudo-random sequence. The pseudo-random sequences are orthogonal to each other for easy identification of transmission source. The fiber transmitter activated under these sequences will generate a designated high-frequency acoustic sinusoidal wave. This could be treated as amplitude modulation. After receivers catch the signals, the demodulation and correlation test could recover the magnitude and time information for each path simultaneously, as shown in Fig. 66.

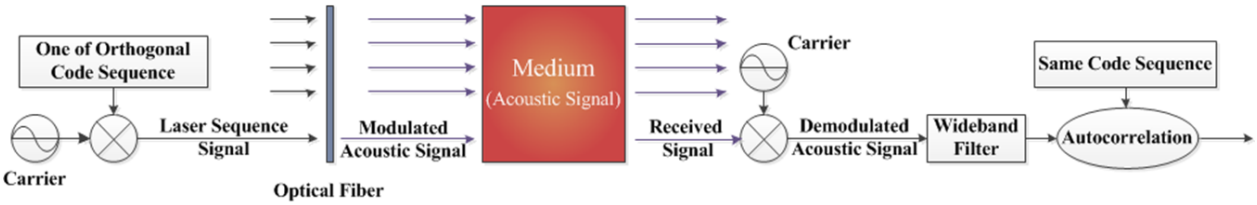

Fig. 66. The diagram of acoustic sensor system based on CDMA scheme.

2) Signal parameters design

Based on the SNR analysis, three parameters are picked as design parameters to achieve desired signal processing performance. They are *f*, the acoustic carrier signal frequency; *L*, number of bits in one address code; and *M*, cycles of carrier signal for on bit of code.

Three performance indices could be evaluated based on *f, L* and *M* as below: 1. The maximum number of channels in this system is equal to *L*; 2. The sampling rate of transition time is equal to *f/LM*, which is different from instrument sampling rate. It's like the system sampling rate to take one transition time measurement; 3. Signal-to-noise ratio (SNR) is proportional to *LM*. With higher SNR, lower uncertainty would be expected at the receiver side.

3) Signals transition time detection simulation

A 2-emitter-1-receiver simulation has been conducted under the structure as shown in Fig. 67. Orthogonal codes in the sequence of 1 and -1 were assigned to different emitters as address codes. The 31-bit address code is used to modulate the activating laser signal. After binary phase-shift keying (BPSK) modulation, the carrier signal represented by sinusoidal was used to simulate the acoustic signals activated by corresponding PN laser signals. At receiver side, acoustic signal would be demodulated first. Then its

sliding correlation with different address codes is conducted and arrival time of signals from different sources would be calculated simultaneously. The longer the code, the higher SNR can be achieved according to the information theory. Various techniques such as sliding windows can be used in the decoding for improved efficiency. In the simulation, SNR = -10dB has been achieved for signal corrupted by background Gaussian noise.

The results are shown in Fig. 67 and Fig. 68. Fig. 67 represents the signals modulation procedure. Row 1 and 2 illustrate address codes of each emitter and laser signals spread by the codes. The last row represents the acoustic signals motivated under the laser signals in row 2.

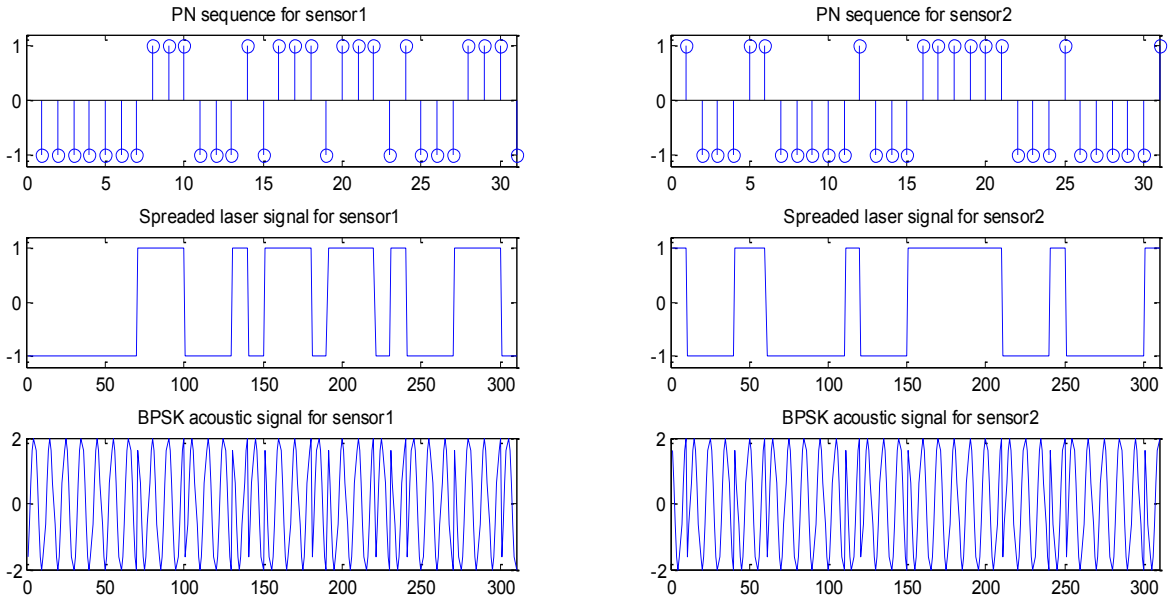

Fig. 67. Modulation for Signals.

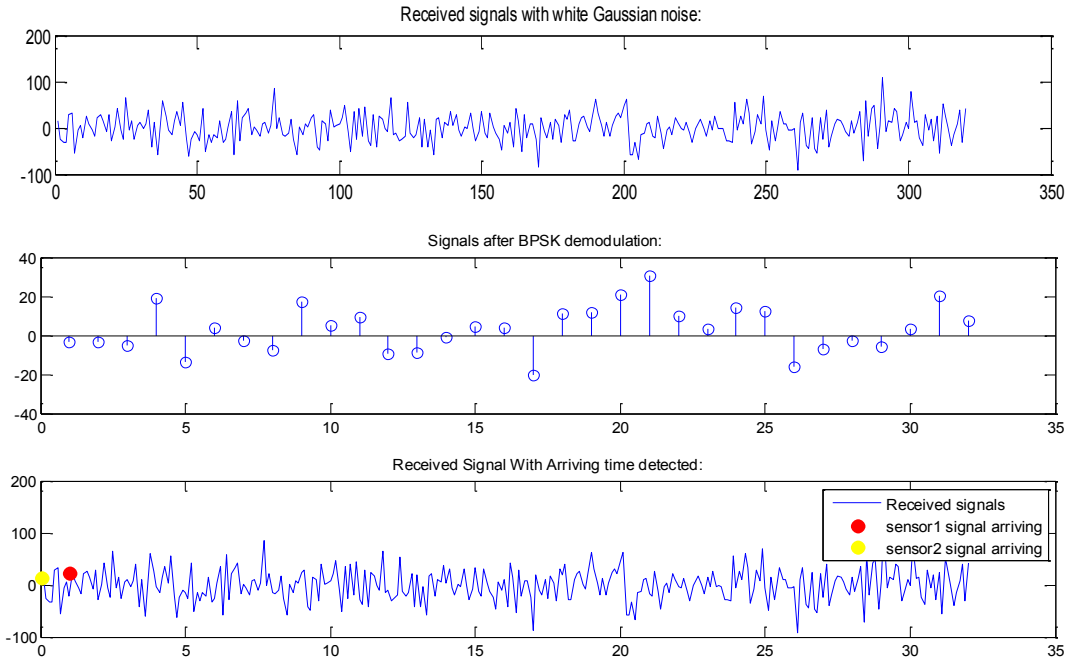

Fig. 68. Demodulation and Transition Time Detection.

The demodulation is shown in Fig. 68. The purpose of sensor system is to accurately measure the different transition time for predetermined paths. Different sensor Ssignals from different sensors should have different arriving time at the receiver end. Thus, in this simulation, each path has been assigned different transition time during transmission. Row 1 shows the mixture signals with additional Gaussian white noise (SNR=-10dB) at receiver end, while row 2 and row 3 show the demodulation process. The sliding correlation calculation has been carried out on the demodulation signal to get all correlative values for each transmitter's address code. The maximum of all these values is the signal arrival time. The figure in row 3 has the arriving time on original receiving signal for two sensors respectively. Compared with predesigned transition time, the system has successfully achieved the arriving time detection.

4) SNR tests

The SNR improvement tests based on length of code was has been also performed based on previous CDMA simulation setup. PN codes with different length were have been tested to see how much SNR that system could allow without losing signal detection accuracy. Table 7 shows the simulation results. The improved performance with increasing code length has verified previous SNR effect analysis.

From literature review, the background noise in a boiler is concentrated in the low frequency band with a sound pressure level (SPL) around 120dB. Thus, from $G_{dB_{signal}} = 20\log_{10}\left(\frac{V_{signal}}{V_0}\right) = 120dB + SNR(dB)$, where V_{signal} is SPL of acoustic signal and V_0 is the standard reference SPL value.

Based on this, the desired sensor signals intensity under specified SNR could be calculated. Table 1 also provides a general guidance for sensor signal design in the future.

Table 7. SNR testing results for different PN codes.

Order N	Length of PN codes ($2^N - 1$)	SNR (dB)	Desired Signal (dB)
5	31	-10	110
6	63	-20	100
7	127	-25	95
8	255	-30	90
9	511	-35	85
10	1023	-40	80

5) Fiber optic sensing system I pilot test signal processing in GE

In this test, the PZT emitting sinusoidal acoustic signals measured from field test in GE are used as experimental data. Then, signal coding is simulated using segments of this data.

The simulation setup is shown as follow, frequency of PZT is $f = 400kHz$. Emitter will be activated twice at time $t = 8ms$ and $t = 16ms$. The background noise is from filed test measurements. The sampling rate of sensor is 50MHz, and signal coding setup are $L = 31$ bits per code and $M = 100$ cycles per bit. Based on the above setup, the system would allow 31 channels multiplexing. The transition time sampling rate is equal to 129Hz. Since the acoustic fiber signal is relatively weaker than PZT signal, the signal's amplitude has been reduced to 0.00015 of original PZT signal in the simulation, and the detection is still work.

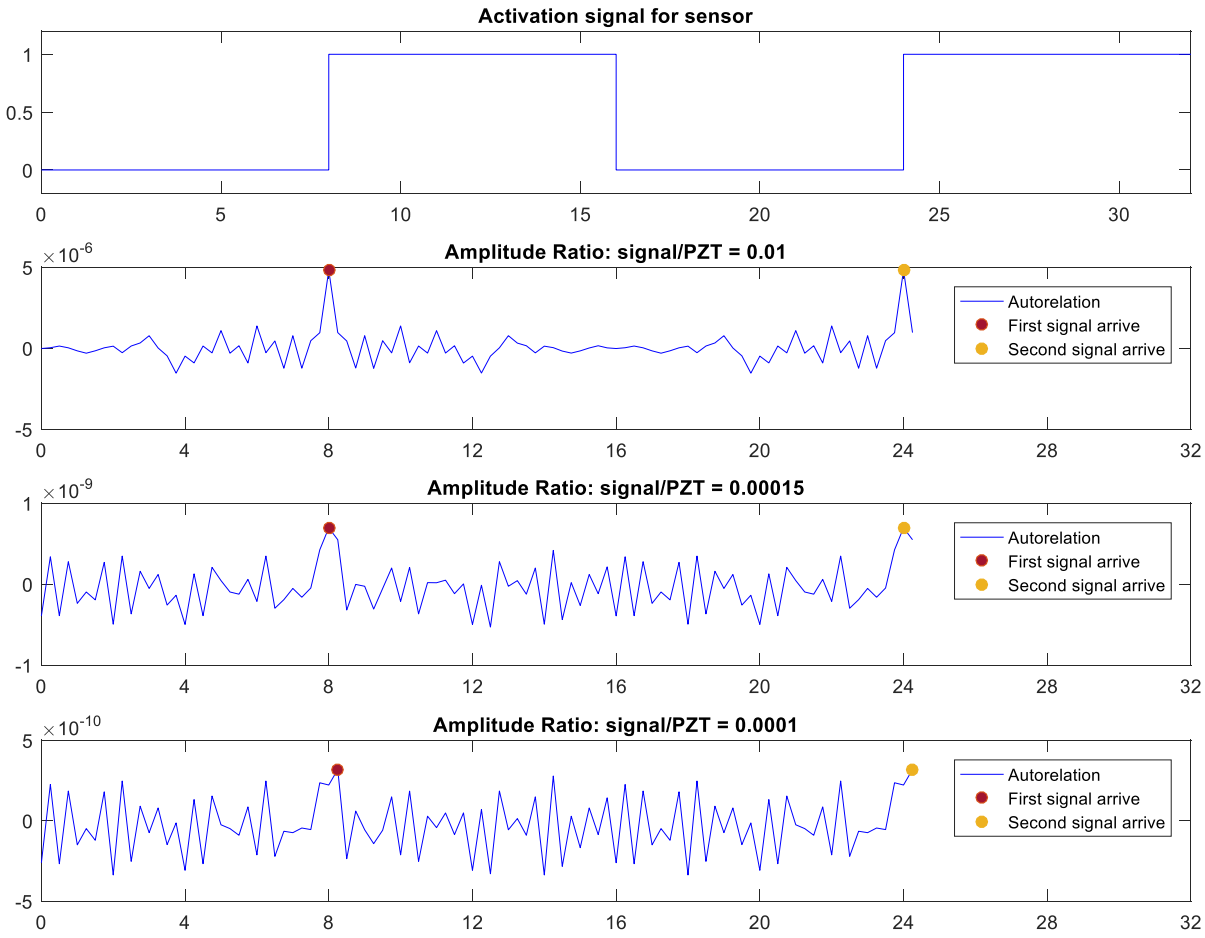

Fig. 69. Comparison for signals with different power intensity.

3.7 Reconstruction algorithm and simulation results (Milestone 2 and Milestone 6)

Reconstruction of 3D temperature field using Neural Networks with measured TOF and known propagation paths is feasible. As we all know, the 3D temperature field is a space distribution profile evolving over time. A general field distribution, even over a compact set, is infinite dimensional in nature. Some sort of spatial discretization or function approximation tools have to be used to transform it into a finite dimensional expression and hence can allow it to be saved, processed or handled by human. Most commonly used spatial discretization tools are polynomial interpolation and functions parameterization. They can formulate the 3D temperature field as truncated series or in a finite dimensional version with residual error. Kernel regression model as one kind of commonly used artificial neural networks (ANN), is a more preferred candidate for function approximation with better efficiency and smaller approximation error. Among various ANNs, GRBF is a good candidate which is a weighted summation of a set of predefined Gaussian functions. GRBF have enjoyed considerable success as basis functions due to innovative features such as high accuracy and exponentially convergence speed. Once the kernel regression model for 3D temperature field reconstruction is built, this will become an inversion problem to solve the best the parameters for the GRBFs. In order to fit the model well with measured data, a cost function which aims to minimize the error between measured data and predicted value is formulated. Gradient descent method will be used for optimizing the cost function in back propagation.

3.7.1 Distributed sensing system

Acoustic pyrometer systems have been used to reconstruct temperature field of a compact set based on measured TOF of sound waves along a number of straight paths. The installation location of emitters/receivers is of great significance to the accuracy of reconstruction. Due to environmental condition constraints, we cannot locate enough emitters/receivers in a given compact set. What's more, although increasing emitters/receivers can improve reconstruction accuracy, in the meanwhile, it leads to higher cost and reduced reconstruction speed. Such trade-off can be achieved with optimized propagation paths. The distribution of emitters/receivers should satisfy the symmetric principle if possible.

Consider a simplified situation where the acoustic signals generated by one sensor can be received by all others. Since TOF is communicative along the same path, N sensors will generate data along $N(N-1)/2$ paths. Effective paths will be less due to non-feasible ones between some sensors. Assume the sensor emits acoustic signals in a sequential manner and each emission/reception takes time T. The total time for a full cycle measurement of $N(N-1)/2$ paths is NT. Since the propagation paths are determined by the location of sensors; it is proposed to design an optimization algorithm for the sensors' distribution. Weights in the 3D space can be assigned depending on the significance of certain locations in the temperature field. Hence, an objective function which integrates the weights along the $N(N-1)/2$ paths can be derived as a function of sensor locations. Maximization of the objective function can be conducted analytically or numerically to extract near optimum distribution of sensors. We can see two typical examples as follows:

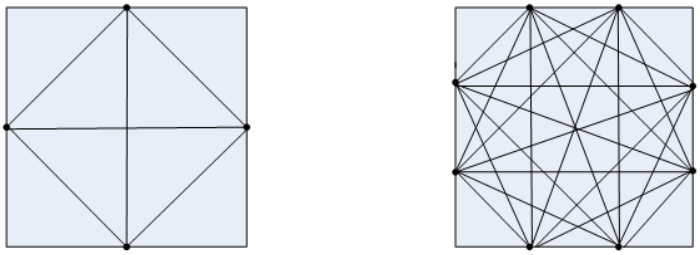

Fig. 70. 4 sensors and 6 paths; 8 sensors and 24 paths.

Suitable sensors and their setup in real world are of great significance to the 3D temperature field reconstruction. For the location of sensors, we should avoid redundant and duplicate paths.

3.7.2 Principle of pyrometer systems

According to the principle of pyrometer system, speed of acoustic waves depends on the temperature of gaseous medium. Hence, the TOF of an acoustic signal over a propagation path can be calculated as:

$$TOF(l_j) = \int \frac{1}{C(x,y,z)} dl_j = \int \frac{1}{Z\sqrt{T(x,y,z)}} dl_j \tag{2}$$

where $C(x,y,z)$ is the velocity of sound at position (x,y,z), Z is the ratio between the specific heats at constant pressure and volume of the gas, and $d(x,y,z)$ is the reciprocal of the sound velocity. Measurements of TOF provide us information about the integral effects of temperature along the pre-defined path between an acoustic emitter and a receiver. To achieve the final objective, the algorithm needs to be designed to derive $d(x,y,z)$ froml_j, $j = 1,2,\cdots$, where M is the number of paths in a full cycle measurement. Once $d(x,y,z)$ is available, temperature field $T(x,y,z)$ can be obtained immediately through a deterministic algebraic relationship.

3.7.3 Reconstruction algorithm

There is no doubt that space discretization has low approximation efficiency and is susceptible to dimension explosion. Regarding Fourier parameterization, it suffers from Gibbs effect and cannot be applied to complex geometries. Compared with space discretization and Fourier series, artificial neural network (ANN) is a more preferred candidate for function approximation with better efficiency and smaller approximation error. Among various ANNs, GRBF is a common choice due to exponentially convergence speed and higher accuracy.

3D temperature field is a space distribution profile evolving over time. A general field distribution, even over a compact set, is infinite dimensional in nature. Because GRBF allows fast convergence and finite elements for problems with complex geometries, it can be used to approximate the temperature field as a finite summation of products of space-dependent basis functions with time-dependent coefficients. A general GRBF always takes the form

$$F(x) = \sum_{i=0}^{N} \omega_i \phi_i = \sum_{i=0}^{N} \omega_i \exp(-(\|x - x_i\|) / 2\sigma^2), \tag{3}$$

where x_i and σ are respectively the center and variance of the Gaussian function. The inversion problem to resolve ω_i is enabled by using gradient descent method.

Following the acoustic pyrometry principle, these Gaussian functions are integrated along a number of known paths which are determined by the distribution of sensors. The inversion problem to estimate the unknown parameters of the Gaussian functions can be resolved with the measured TOF of acoustic waves and the length of propagation paths. The temperature field can be approximated as follows using the GRBF-based parameterization:

$$t_k = \int_{l_k} (Z\sqrt{T(x,y,z)})^{-1} dl_k = \frac{1}{Z} \int_{l_k} \sum_{i=1}^{M} \omega_i g_i(x,y,z) dl_k \qquad (1 \le k \le N) \tag{4}$$

$$\begin{aligned} & (\sqrt{T(x,y,z)})^{-1} \\ &= \sum_{i=1}^{M} \omega_i g_i(x,y,z) \\ &= \sum_{i=1}^{M} \omega_i \cdot \exp\{-[(x-X_i)^2 + (y-Y_i)^2 + (z-Z_i)^2] / 2\sigma^2\} (1 \le i \le M) \end{aligned} \tag{5}$$

where l_k is the integral path, N is the number of propagation paths which is decided by sensors, M is the number of Gaussian Functions.

3.7.4 2D and 3D temperature field simulation results

Simulation results of 2D and 3D temperature field reconstruction are shown in Fig. 71 - Fig. 74. For the 2D plane with 10×8 area, 10 sensors were evenly distributed, 10 basis functions were used and 24 paths were chosen. For the 3D field with 2×2×0.8 space, 24 sensors are evenly distributed, 30 basis functions are used and 276 paths were chosen. Reconstruction of unimodal symmetric and unimodal deflection temperature field are demonstrated below.

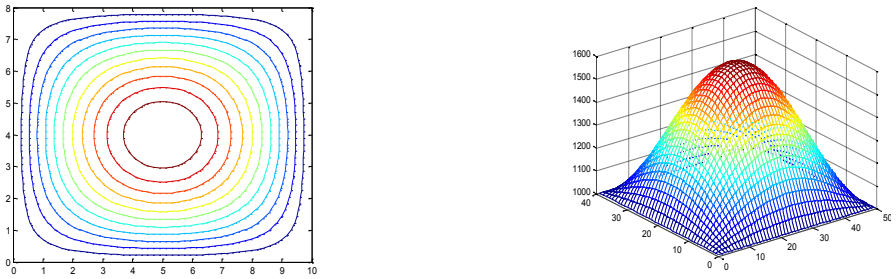

(a) Contour and mesh of real temperature field

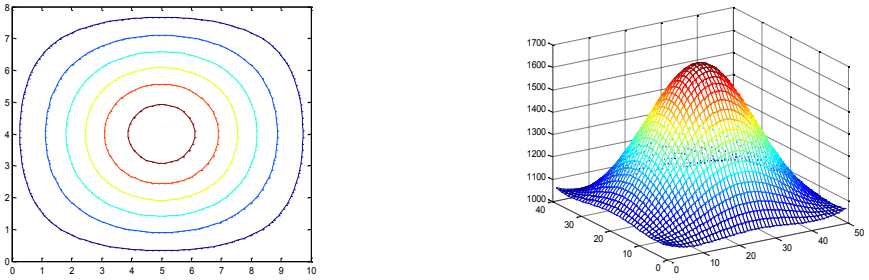

(b)Contour and mesh of reconstructed temperature field

Fig .71. Unimodal symmetric temperature field $T(x, y) = 1000 + 600\sin(\pi x / length)\sin(\pi y / height)$.

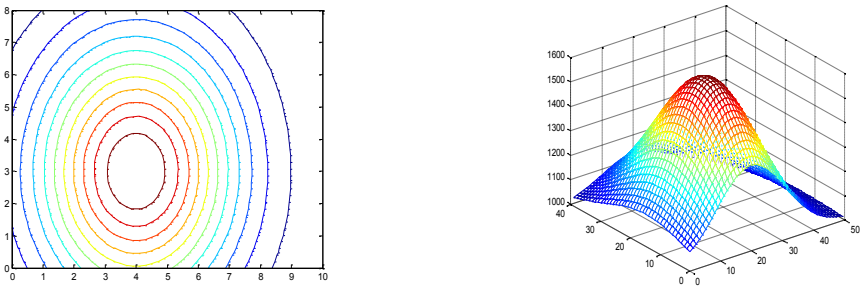

(a) Contour and mesh of real temperature field

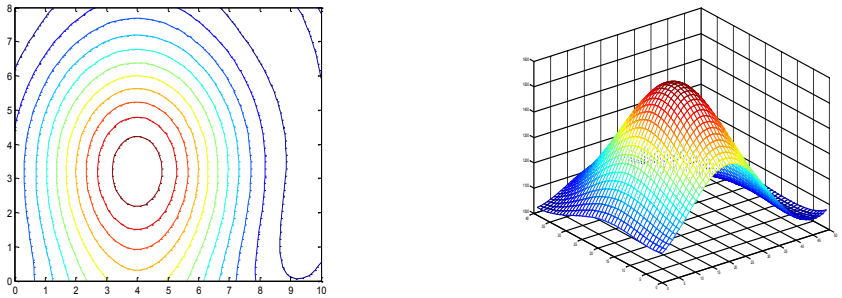

(b)Contour and mesh of reconstructed temperature field

Fig.72. Unimodal deflection temperature field $T(x, y) = 600\exp((-(x-4)^2)/length - ((y-3)^2)/(2*height)) + 1000$

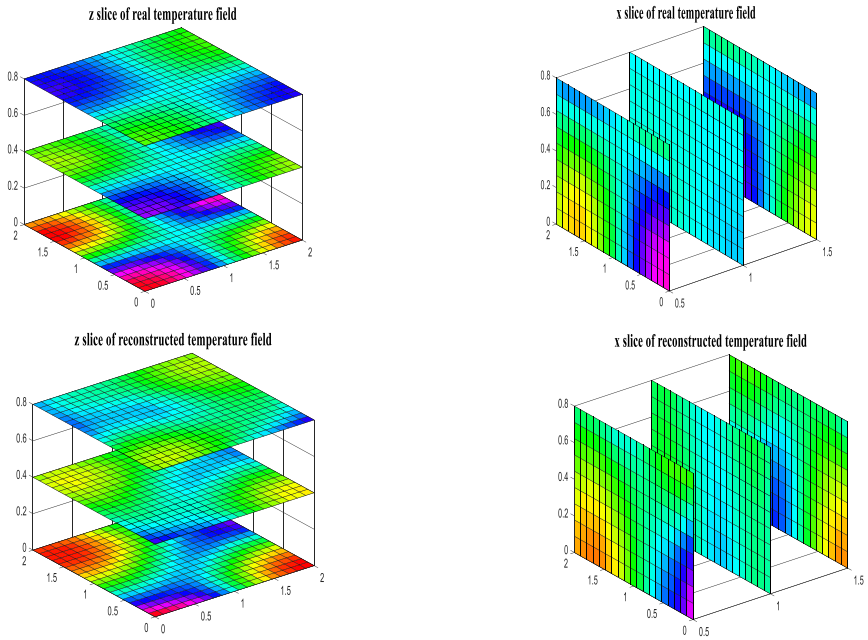

Fig.73. 3D temperature field $T(x, y, z) = 100 + 500\cos(1.5x)\cos(2y)\cos(2.5z)$.

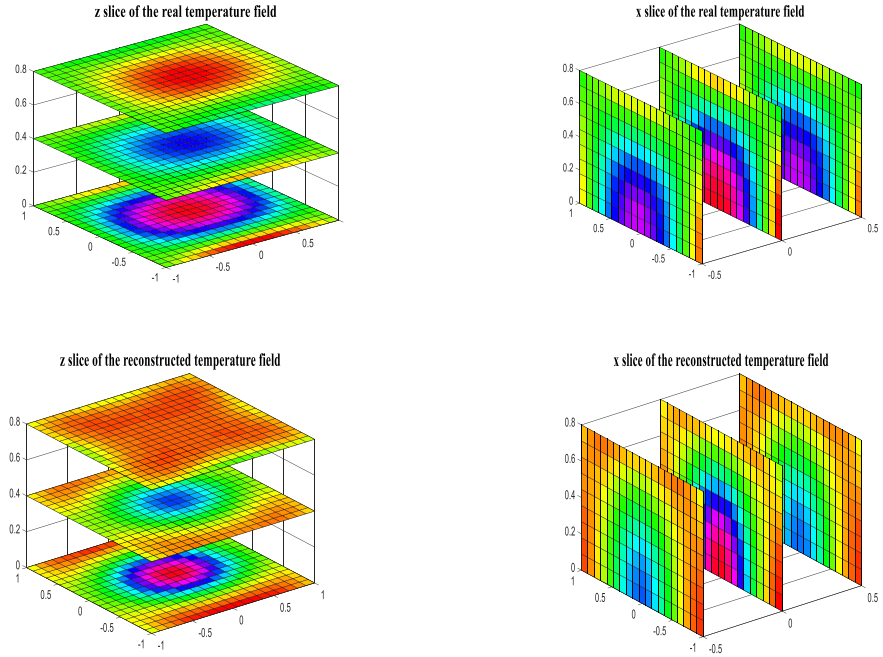

Fig.74. 3D temperature field $T(x, y, z) = 800 + 600\cos(x - 0.3)\cos(2y - 0.4)\cos(1.5z)$

3.7.5 Data analysis

1) Design parameter

The number N of basis functions we choose plays an important role in the accuracy of reconstruction. The Table 8 below is the simulation results for different choice of N.

Table 8. Reconstruction error with different choice of *N*

N	5	6	7	8	9	10
Average absolute error (°C)	81.31	28.57	27.63	27.14	25.28	26.60
Average relative error (%)	6.94	2.53	2.46	2.21	2.19	2.18

As we can see from Table 8, larger N leads to both smaller average absolute error and average relative error; however, benefits will decrease as N increases.

2) Initial uncertainty analysis

Suppose N is the number of basis functions, and M is the number of paths.

Without measurement noise, we have

$$\int \sum_{i=1}^{N} \omega_i \phi_i(x,y,z) dl_j = t_j \qquad (i = 1,...,N; j = 1,...,M)$$

which can also be written as

$$\begin{bmatrix} \int \phi_1(x,y,z)dl_1 & \cdots & \int \phi_i(x,y,z)dl_1 & \cdots & \int \phi_N(x,y,z)dl_1 \\ \vdots & & \vdots & & \vdots \\ \int \phi_1(x,y,z)dl_j & \cdots & \int \phi_i(x,y,z)dl_j & \cdots & \int \phi_N(x,y,z)dl_j \\ \vdots & & \vdots & & \vdots \\ \int \phi_1(x,y,z)dl_M & \cdots & \int \phi_i(x,y,z)dl_M & \cdots & \int \phi_N(x,y,z)dl_M \end{bmatrix} \begin{bmatrix} \omega_1 \\ \vdots \\ \omega_i \\ \vdots \\ \omega_N \end{bmatrix} = \begin{bmatrix} t_1 \\ \vdots \\ t_j \\ \vdots \\ t_M \end{bmatrix} \tag{6}$$

With measurement noise, we have

$$\int \sum_{i=1}^{N} \overline{\omega}_i \phi_i(x,y,z) dl_j = t_j + \Delta t_j \qquad (i = 1,...,N; j = 1,...,M)$$

which can also be written as

$$\begin{bmatrix} \int \phi_1(x,y,z)dl_1 & \cdots & \int \phi_i(x,y,z)dl_1 & \cdots & \int \phi_N(x,y,z)dl_1 \\ \vdots & \vdots & \vdots & \vdots & \vdots \\ \int \phi_1(x,y,z)dl_j & \cdots & \int \phi_i(x,y,z)dl_j & \cdots & \int \phi_N(x,y,z)dl_j \\ \vdots & \vdots & \vdots & \vdots & \vdots \\ \int \phi_1(x,y,z)dl_M & \cdots & \int \phi_i(x,y,z)dl_M & \cdots & \int \phi_N(x,y,z)dl_M \end{bmatrix} \begin{bmatrix} \bar{\omega}_1 \\ \vdots \\ \bar{\omega}_i \\ \vdots \\ \bar{\omega}_N \end{bmatrix} = \begin{bmatrix} t_1 + \Delta t_1 \\ \vdots \\ t_j + \Delta t_j \\ \vdots \\ t_M + \Delta t_M \end{bmatrix} \tag{7}$$

It can be noticed from (6) and (7) that measurement noise in travelling time will propagate into the integral process for reconstruction. The simulation results in Fig. 75 demonstrate the effects of measurement noise existing in travelling time on the reconstruction accuracy.

After calculation, the maximum absolute error is 91.98 °C, the average absolute error is 17.23 °C, the maximum relative error is 8.82%, and the average relative error is 1.47%.

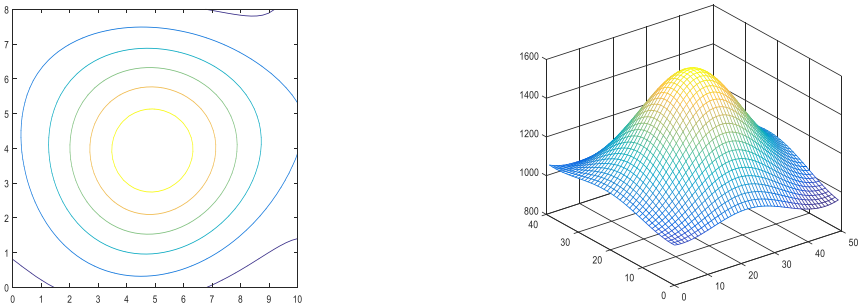

(a)Reconstruction with measurement noise.

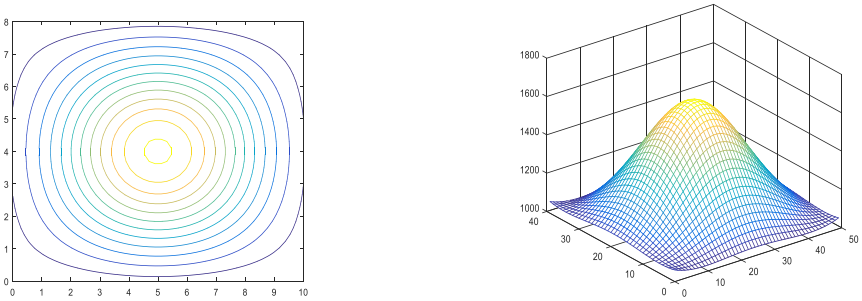

(b)Reconstruction without measurement noise.

Fig.75. Effects of measurement noise existing in travelling time on the reconstruction accuracy.

4 Students support, Published papers, Patents and Potential licenses

Students support:

Postdoc Researchers: Nan Wu (2014-2016, hired at Philips), Poorna Marthi (2018, hired at Intel)
Ph.D. Students: Jingcheng Zhou, Xu Guo, Cong Du, Tong Ma and Yuqian Liu
Master Students: Siwen Bi (2014- 2015, hired at UMass Lowell Plastic Engineering as a Ph.D. student) and Rachana Guruprasad Kashyap

Published papers:

[1] Jingcheng Zhou, Nan Wu, Xingwei Wang, Yuqian Liu, Tong Ma, Daniel Coxe, Chengyu Cao, "Water temperature measurement using a novel fiber optic ultrasound transducer system", IEEE International Conference on Information and Automation, Lijiang, China, August 8-10, 2015.

[2] Tong Ma, Yuqian Liu, Chengyu Cao, Jingcheng Zhou, Nan Wu, Xingwei Wang, "3D Reconstruction of Temperature Field Using Gaussian Radial Basis Functions (GRBF)", IEEE International Conference on Information and Automation, Lijiang, China, August 8-10, 2015.

[3] Xu Guo, Nan Wu, Yunhan Luo, Zhe Chen, Xingwei Wang, "Ultrasound generation from a side-polished optical fiber", ISFA 2016, Cleveland, Ohio, USA, August 1-3, 2016.

[4] Jingcheng Zhou, Nan Wu, Tong Ma, Xu Guo, Cong Du, Yuqian Liu, Chengyu Cao, Xingwei Wang, "Proof of concept temperature field monitoring using optically generated acoustic waves sensing", 59th ISA POWID Symposium, Charlotte, North Carolina USA, June 27-30, 2016.

[5] Yuqian Liu, Tong Ma, Chengyu Cao, Xingwei Wang, "3D temperature field reconstruction using ultrasound sensing system", Proceedings of SPIE, 98030V, 2016.

[6] Siwen Bi, Nan Wu, Jingcheng Zhou, Qixiang Tang, Jones Owusu Twumasi, Tzuyang Yu, Xingwei Wang, "Ultrasonic transmission from fiber optic generators on steel plate", Proceedings of SPIE, 98040Q, 2016.

[7] Siwen Bi, Nan Wu, Jingcheng Zhou, Tong Ma, Yuqian Liu, Chengyu Cao, Xingwei Wang, "Ultrasonic temperature measurements with fiber optic system", Proceedings of SPIE, 98031Y, 2016.

[8] Siwen Bi, Nan Wu, Jingcheng Zhou, Haifeng Zhang, Chen Zhang, Xingwei Wang, "All-optically driven system in ultrasonic wave-based structural health monitoring", Proceedings of SPIE, 98030K, 2016.

[9] Jingcheng Zhou, Nan Wu, Siwen Bi, Xingwei Wang, "Ultrasound generation from an optical fiber sidewall", Proceedings of SPIE, 98031U, 2016.

[10] Xu Guo, Xingwei Wang, Nan Wu, Jingcheng Zhou and Cong Du, "Ultrasound generation from side wall of optical fibers" ICOCN 2017, Wuzhen, China, Aug 7-10, 2017. (Invited talk)

[11] Jingcheng Zhou, Nan Wu, Xu Guo, Cong Du, Carl Edberg, Xinsheng Lou, Tong Ma, Yuqian Liu, Chengyu Cao, Xingwei Wang, "A fiber optic ultrasound transducer system for high temperature measurement in a boiler" 60th ISA POWID Symposium, Cleveland, Ohio USA, June 26-29, 2017.

[12] Jingcheng Zhou, Xu Guo, Cong Du, Poorna Marthi, Tong Ma, Yuqian Liu, Carl Edberg, Xinsheng Lou, Chengyu Cao and Xingwei Wang,"Ultrasonic wave-based all optical fiber sensor system for high temperature monitoring in a boiler" 2018 ISA POWID Symposium, Knoxville, Tennessee, USA, 26-28, June 2018

[13] Jingcheng Zhou, Xu Guo, Cong Du, Nan Wu, Xingwei Wang, "Characterization of ultrasonic generation from a fiber-optic sidewall" SPIE Defense + Commerical sensing, Orlando, Florida, United States, 15-19, April 2018

[14] Jingcheng Zhou, Xu Guo, Cong Du, Nan Wu, Xingwei Wang, "High temperature monitoring using a novel fiber optic ultrasonic sensing system" SPIE Defense + Commerical sensing, Orlando, Florida, United States, 15-19, April 2018

[15] Jingcheng Zhou, Xu Guo, Cong Du, Chengyu Cao, Xingwei Wang. "A Fiber Optic Ultrasonic Sensing System for High Temperature Monitoring Using Optically Generated Ultrasonic Waves." Sensors 19, no. 2 (2019): 404.

Patents:

[1] The In Situ Monitoring Equipment of Multi Characteristic Parameters of Gas; 28-Jul-17 Xu Guo; Tongyu Liu; Xingwei Wang *; Yin Wang; Yubin Wei; Jingcheng Zhou ; Case Active - Application Filed

[2] Fiber optic temperature measurement system 23-Mar-15 Xingwei Wang *; Nan Wu 62/170,764; PCT/US2016/035748; 15/569,113; Case Active - Application Filed

[3] Distributed fiber sensing systems for temperature field monitoring using optically generated acoustic waves 17-Jul-14 Xingwei Wang *; Nan Wu 62/155,796; PCT/US2016/030074; 15/569,112; EP-tbd; IN-tbd; CA-tbd Department of Energy; Case Active - Application Filed

Potential licenses:

A company, TESSSO, would like to option our technology for licensing.

5 Conclusions

This project aims to develop a fiber optic sensing system to conduct temperature measurement in high temperature environments. Three kinds of three fiber optic sensing systems for boiler temperature measurement have been developed and tested. The project made the gap closer between the fundamental researches of using optical fibers to do 3D boiler temperature reconstruction. For fiber optic sensing system I, we got 2D temperature reconstruction results and it matched the reference data. It successfully survived in GE ISBF boiler environment (480 °F). For fiber optic sensing system II, it not only survived at up to 700°C furnace environment and 320 °C GE ISBF boiler environment, but also clearly detected the boiler temperature information. For fiber optic sensing system III, it successfully survived at room temperature in GE ISBF boiler wind condition. We have not only carried out a lot of experiments, but also carried out simulation and algorithm optimization. The CDMA modulation technique has been proposed and studied to guarantee high network throughput, low channel access delay and low energy consumption. 2D and 3D temperature field reconstruction simulation results are achieved. The successful accomplishment of this project established a foundation of the prototype of the Fiber Optic Sensing System and will attract more attention from companies and funding.

In this project, we have finished most of the tasks as we proposed in the proposal. We finished milestone 1-8 and milestone 10. For milestone 9, we conducted three pilot tests using the fiber optic sensing system III (Distributed Sensing System II) at GE Power, but due to the failure of the ns laser, we did not get the high temperature measurement results. We also performed some additional tasks which were not in the original proposal: 1) We fabricated a fiber optic sensing system I and did a pilot test based on this system. 2) In the proposal, we proposed two pilot tests at GE Power. In reality, we finished at least seven pilot tests at GE Power. GE Power has made a lot of efforts for supporting the pilot tests. 3) We got a simulation results based on CDMA.

In the future, when additional funding is available, we will increase the testing distance of the fiber optic sensing system II and III. We will increase the fiber generator signal strength. Based on fiber optic sensing system I distance test results, we can find the fiber optic ultrasound generator has the potential for long distance pilot test. We will also increase the testing temperature of the optical sensing system. Right now, the highest measured temperature is 700 degrees C by using fiber optic sensing system II. We will try to use special fibers (such as gold-coated fiber and sapphire fiber) to improve the design of our fiber optic sensing system. By using the special materials, the whole optical sensing system could survive in the much higher temperature environment (> 700 degrees C).

In this project, 9 students were supported, 15 paper were published, 3 patents were submitted and 1 company contacted us for a possible technology licensing. Two journal papers are under preparation and will be submitted.

Acknowledgement

This project supported by the U.S. Department of Energy under Award No. DE-FE0023031. First of all, we are thankful to the Department of Energy and our project manager, Barbara Carney and Jessica Mullen. We would like to express our sincere thanks towards Prof. Siman Li, Dr. Yin Wang at UML and Prof. Zixue Luo at UConn as visiting scholars for helping our work. Nevertheless, we would like to express our sincere thanks towards Dr. Junwei Su and Che-fu Su at UML Mechanical Engineering Department for assisting in machining problems.

We are grateful to Mr. Carl Edberg and his test team at General Electric for supporting the pilot tests. We also thank Mr. Ray Chamberland for his support on the UML-GE contract agreement.